

# Learning Credal Ensembles via Distributionally Robust Optimization

Kaizheng Wang<sup>\*1, 2</sup>, Ghifari Adam Faza<sup>4, 5</sup>, Fabio Cuzzolin<sup>3</sup>, Siu Lun Chau<sup>2</sup>,  
 David Moens<sup>4, 5</sup>, and Hans Hallez<sup>1</sup>

<sup>1</sup>Department of Computer Science, KU Leuven, Belgium

<sup>2</sup>College of Computing and Data Science, Nanyang Technological University, Singapore

<sup>3</sup>School of Engineering, Computing, and Mathematics, Oxford Brookes University, U.K.

<sup>4</sup>Department of Mechanical Engineering, KU Leuven, Belgium

<sup>5</sup>Flanders Make@KU Leuven, Belgium

February 10, 2026

## Abstract

Credal predictors are epistemic-uncertainty-aware models that produce a convex set of probabilistic predictions. They provide a principled framework for quantifying predictive epistemic uncertainty (EU) and have been shown to improve model robustness across a range of settings. However, most state-of-the-art (SOTA) methods primarily define EU as disagreement induced by random training initializations, which mainly reflects sensitivity to optimization randomness rather than uncertainty from more substantive sources. In response, we formulate EU as disagreement between models trained under different degrees of relaxation of the i.i.d. assumption between the training and test distributions. Building on this idea, we propose *CreDRO*, which learns an ensemble of plausible models via distributionally robust optimization. As a result, CreDRO captures EU arising not only from training randomness but also from informative disagreement due to potential train–test distribution shifts. Empirically, CreDRO consistently outperforms SOTA credal approaches on downstream tasks, including out-of-distribution detection on extensive benchmarks and selective classification in medical settings.

Keywords: Uncertainty Quantification, Epistemic Uncertainty, Credal Sets, Classification

## 1 Introduction

Quantifying predictive uncertainty in deep neural networks (NNs) has become increasingly important, as reliable uncertainty quantification (UQ) is essential for improving the robustness and trustworthiness of machine learning systems, particularly in safety-critical applications [Zhou et al., 2012, Mehrtens et al., 2023, Wang et al., 2026]. However, informative UQ requires distinguishing aleatoric uncertainty (AU), which stems from inherent randomness in the data-generation process, from epistemic uncertainty (EU), which arises from NNs’ limited knowledge about the true input-output relationship [Hüllermeier and Waegeman, 2021]. These two forms of uncertainty have fundamentally different implications for downstream decision-making. In particular, reliable estimation of EU is beneficial for tasks where utilizing model’s predictive confidence is crucial, such as in selective prediction [Shaker and Hüllermeier, 2021b, Chau et al., 2025a], learning to reject and

---

\*The main part of this work was conducted at KU Leuven and completed at Nanyang Technological University.

defer [Liu et al., 2022], Bayesian optimization [Tuo and Wang, 2022], and out-of-distribution (OOD) detection [Mucsányi et al., 2024].

Unlike AU, which is usually modeled by a single (conditional) probability distribution (e.g., via a softmax probabilistic prediction in classification), EU generally requires a second-order formalism to represent uncertainty about the model’s (probabilistic) prediction itself [Hüllermeier and Waegeman, 2021, Wang et al., 2026]. Under this context, credal sets [Levi, 1980], i.e., convex sets of probability distributions, serve as an appealing second-order representation of uncertainty over first-order probabilistic predictions [Zaffalon, 2002, Corani and Zaffalon, 2008, Corani et al., 2012, Mauá et al., 2017], and have inspired recent advances to improve EU quantification in deep learning. For instance, a recent credal wrapper approach [Wang et al., 2025b] formulates credal set predictions from multiple softmax outputs of a deep ensemble [Lakshminarayanan et al., 2017] trained with different random initializations. In addition, a credal ensembling method [Nguyen et al., 2025] is proposed as an alternative post hoc extension to a classical ensemble. This method also allows discarding outlier probabilities through a hyperparameter  $\alpha$ , preventing credal sets from becoming too large. Moreover, Löhr et al. [2025] introduce a scheme that increases ensemble diversity and selects plausible members using a predefined threshold based on the concept of relative likelihood. See Appendix A for an extended literature review. Although these credal predictors have been shown to improve model robustness across a range of classification settings, they capture EU as disagreement induced by random training initializations, mainly reflecting the sensitivity to optimization randomness rather than uncertainty from more substantive sources.

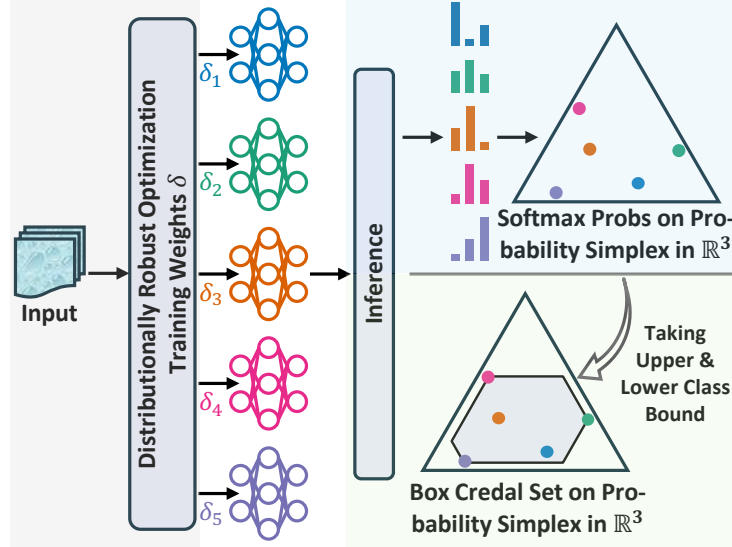


**Figure 1:** CreDRO Concept. ① Training: An ensemble is trained using distributionally robust optimization with members weighted differently to simulate varying degrees of train-test distribution shifts (see Section 3.1). ② Inference: Softmax probabilities are converted into class-wise probability intervals, creating a box credal set (see Section 3.2).

**Contributions.** In response, we formulate EU as disagreement among ensemble member models trained under different degrees of relaxation of the i.i.d. assumption between the training and test distributions. Following this principle, we propose *CreDRO*, which learns an ensemble of plausible models using distributionally robust optimization (DRO) by varying a hyperparameter to simulate different degrees of potential train–test distribution shift.

As a result, CreDRO captures not only training randomness but also informative disagreement arising from potential train–test distribution shifts. At inference time, CreDRO transforms individual softmax probabilities from the ensemble into class-wise probability intervals [De Campos et al., 1994], and uses them to form a box credal set [Wang et al., 2025b] prediction, i.e., a set of probabilities confined by the intervals. The concept of CreDRO is illustrated in Figure 1.

Compared to state-of-the-art (SOTA) credal classifiers and the deep ensemble baseline, CreDRO consistently achieves superior epistemic uncertainty (EU) quantification performance across multiple out-of-distribution (OOD) detection and selective classification benchmarks. This indicates that distributionally robust optimization (DRO) yields substantially higher-quality epistemic uncertainty estimates than those obtained from random model initializations.

**Further related work.** In addition to ensemble and credal predictors, Bayesian neural networks (BNNs) [Blundell et al., 2015, Gal and Ghahramani, 2016, Krueger et al., 2017, Mobiny et al., 2021] and evidential deep learning (EDL) [Malinin and Gales, 2018, 2019, Charpentier et al., 2020] are alternative second-order approaches. However, BNNs often face practical limitations, including scalability issues with large datasets or complex model architectures and the need for many forward passes [Mukhoti et al., 2023]. EDL has also attracted recent criticism [Bengs et al., 2023, Juergens et al., 2024, Shen et al., 2024]. In particular, EDL may fail to represent EU faithfully. For example, Juergens et al. [2024] show that confidence bounds derived from EDL’s EU estimates differ substantially from those of the reference distribution, which is defined as the distribution of the first-order predictor induced by the training data sampling process and is used to assess EU quantification quality. Singh et al. [2024] have proposed imprecise learning to consider all possible DRO constraints by solving an infinite-objective optimization, instead of retaining the uncertainty through an ensembling approach.

**Paper outline.** The rest of this paper is organized as follows. Section 2 provides the background of DRO and deep ensembles. Section 3 introduces our CreDRO in full detail. Section 4 describes experimental validation. Section 5 summarizes the conclusion and future work.

## 2 Preliminaries

### 2.1 Distributionally robust optimization (DRO)

In supervised learning, a neural network (NN) with trainable parameters, denoted as  $h_\theta(\cdot)$ , is generally trained on a set of labeled samples  $\{\mathbf{x}_n, y_n\}_{n=1}^N$ . One standard approach is the empirical risk minimization (ERM) framework, where the parameter  $\theta$  is obtained by solving

$$\underset{\theta}{\text{minimize}} \left\{ \frac{1}{N} \sum_{n=1}^N \mathcal{L}((h_\theta(\mathbf{x}_n), y_n)) \right\}, \quad (1)$$

where  $\mathcal{L}(\cdot, \cdot)$  is a chosen loss function. However, the ERM often yields over-optimistic predictions during deployment because it assumes the training and test distributions are identical—an assumption that frequently fails in practice, where test data can differ significantly from the training samples [Huang et al., 2022].

To improve the robustness of NNs to distribution discrepancies, the DRO framework relaxes the i.i.d. assumption between the training and test distributions by assuming that the future test distribution lies within a neighborhood of the training distribution  $P$ . Under this context, the DRO framework minimizes a worst-case expected risk  $R(\theta)$  over an uncertain set of distributions  $\mathcal{U}$  [Ben-Tal et al.,

2013, Oren et al., 2019, Duchi et al., 2021].

$$\underset{\theta}{\text{minimize}} \left\{ R(\theta) \doteq \sup_{P \in \mathcal{U}} \mathbb{E}_{(\mathbf{x}, y) \sim P} \mathcal{L}(h_{\theta}(\mathbf{x}), y) \right\}. \quad (2)$$

To make the DRO framework practical, *group DRO* methods have been proposed [Oren et al., 2019, Sagawa et al., 2019]. These approaches assume the training distribution  $P$  is a mixture of  $m$  groups  $P_g$ , indexed by  $g \in \mathcal{G} = \{1, \dots, m\}$ . Since the optimum of a linear program occurs at a vertex, the worst-case risk  $R(\theta)$  in (2) simplifies to maximizing the expected loss over each group, with the training objective:

$$\underset{\theta}{\text{minimize}} \left\{ \underset{g \in \mathcal{G}}{\text{maximize}} \mathbb{E}_{(\mathbf{x}, y) \sim P_g} \mathcal{L}(h_{\theta}(\mathbf{x}), y) \right\}. \quad (3)$$

A remaining practical challenge in implementing (3) lies in constructing an empirical estimate of the distribution  $P_g$  for each group when only limited training data are available.

In response, *adversarially reweighted learning*—a specific form of *group DRO* [Sagawa et al., 2019, Lahoti et al., 2020, Nam et al., 2020]—has been adopted. Specifically, (3) is implemented as a minimax game between a learner and an adversary. The learner optimizes parameters  $\theta$  to minimize the expected loss whereas the adversary maximizes the expected loss by adversarially assigning the sample with weights  $w_n$ , collected in a vector  $\mathbf{w}$ . The resulting training objective becomes:

$$\underset{\theta}{\text{minimize}} \left\{ \underset{\mathbf{w} \in \mathbb{W}}{\text{maximize}} \frac{1}{N} \sum_{n=1}^N w_n \mathcal{L}(h_{\theta}(\mathbf{x}_n), y_n) \right\}, \quad (4)$$

The predefined set of weight vectors  $\mathbb{W}$  is a subjective design choice due to the lack of knowledge about the actual test distribution, and has been defined in various ways, see Lahoti et al. [2020], Nam et al. [2020], Sagawa et al. [2019], Wang et al. [2024].

## 2.2 Deep ensembles

Deep ensembles (DE) have demonstrated significant advantages in quantifying prediction uncertainty by independently training multiple randomly-initialized neural networks [Lakshminarayanan et al., 2017]. Specifically, a DE consists of a set of classical neural networks  $\{h_{\theta_i}(\cdot)\}_{i=1}^M$  with probabilistic predictions. This is the default setup used throughout the paper unless otherwise noted. For classification, each network produces individual softmax probabilities  $\{\mathbf{p}_i\}_{i=1}^M$  at inference time.

To make a final precise prediction, a DE takes the averaged probability vector  $\tilde{\mathbf{p}} = M^{-1} \sum_{i=1}^M \mathbf{p}_i$ . EU is quantified by using the well-known *approximate mutual information* [Hüllermeier and Waegeman, 2021], as follows:

$$\sum_{k=1}^C -\tilde{p}_k \log \tilde{p}_k - \frac{1}{M} \sum_{i=1}^M \sum_{k=1}^C -p_{i,k} \log p_{i,k}. \quad (5)$$

Here,  $\tilde{p}_k$  denotes the  $k$ -th element of the averaged probability vector  $\tilde{\mathbf{p}}$ . The expression for epistemic uncertainty in (5) arises from the standard decomposition of total predictive uncertainty into aleatoric and epistemic components [Hüllermeier and Waegeman, 2021]. In this setting, EU encoded in the Bayes framework [Hüllermeier et al., 2022] reflects an ensemble’s disagreement induced by random training initializations.

DEs have long served as a strong baseline for UQ in deep learning. Several variants—such as batch ensembles [Wen et al., 2020], masked ensembles [Durasov et al., 2021], and packed ensembles [Laurent et al., 2022]—have been proposed to provide uncertainty estimates comparable to those of standard DEs, while significantly improving computational efficiency. However, these variants differ from

our primary focus, which is to prioritize further improvements in uncertainty quantification—a consideration that is particularly critical in safety-critical applications. More recently, the credal wrapper [Wang et al., 2025b] has demonstrated that mapping deep ensemble predictions into a credal framework can substantially improve the resulting epistemic uncertainty (EU) quantification. Nevertheless, the uncertainty captured by this post-hoc transformation remains fundamentally tied to the same source of variability, namely, ensemble disagreement arising from random training initializations.

### 3 Main method: CreDRO

This section details our CreDRO framework. Section 3.1 introduces how CreDRO is trained by the DRO strategy, and Section 3.2 presents the credal prediction generation and its EU qualification.

#### 3.1 Training procedure

The CreDRO method constructs an ensemble of plausible probabilistic models, each trained under a different degree of potential train–test distribution shift. The resulting disagreement among these models reflects epistemic uncertainty about the prediction at deployment, in contrast to classical ensemble disagreement arising solely from different random model initializations.

Methodologically, we adopt the adversarially reweighted learning (ARL) framework in (4) from the *group DRO* family (see Section 2.1). Our method enables standard batch-wise optimization for NN training under the ARL framework while encouraging each network to specialize in different group distributions. As a result, the CreDRO produces diverse probabilistic predictions that reflect a range of different degrees of relaxation of the i.i.d. assumption between train-test distributions. In the following, we first describe our implementation of the DRO strategy for a single model, and then present the ensemble training procedure.

**A flexible ARL-based DRO implementation.** To avoid the inefficiency of directly estimating the weights  $\mathbf{w}$  in (4) under the standard batch-wise NN training, CreDRO adopts a flexible approximation scheme inspired by Huang et al. [2022], Wang et al. [2024]. Specifically, during batch-wise training, only the top  $\delta$  portion of samples with the highest loss values in each batch are used for backpropagation [Huang et al., 2022]. Under this scheme,  $w_n > 1$  is implicitly assigned to the selected high-loss samples, while  $w_n = 0$  is assigned to the remaining samples in (4). The underlying rationale is that these hard-to-learn instances may correspond to minority groups within the training data, thereby simulating potential domain shifts at test time [Huang et al., 2022].

**CreDRO ensemble training.** In the proposed scheme, a particular choice of  $\delta$  represents a hypothesized level of discrepancy between the train-test distributions. To build an end-to-end CreDRO framework—i.e., an ensemble of plausible members that encode varying degrees of assumptions about possible distribution shifts—we introduce a global, user-defined hyperparameter  $\delta_G \in [0.5, 1)$  that reflects the assumed worst-case divergence. The value of  $\delta_i$  used to train the  $i$ -th individual model is then:

$$\delta_i = \frac{(1 - \delta_G)}{(M - 1)} \cdot (i - 1) + \delta_G, \quad (6)$$

which corresponds to a uniform interpolation over  $[\delta_G, 1]$ . The lower bound of the design range for  $\delta_G$  is set to 0.5. This is because an overly small  $\delta_G$  implies training focuses on a few high-loss samples, causing large average loss values for gradient updates during backpropagation, leading

---

**Algorithm 1** Batch-wise CreDRO Training Procedure

---

**Input:** Training batch data  $\{\mathbf{x}_n, y_n\}_{n=1}^\eta$ ; hyperparameter  $\delta_G \in [0.5, 1)$ ; batch size  $\eta$ ; ensemble size  $M$

**Output:** Trained  $M$  single models  $\{h_{\theta_i}\}_{i=1}^M$

**for**  $i = 1, \dots, M$  **do**

1. Calculate loss  $\mathcal{L}(h_{\theta_i}(\mathbf{x}_n), y_n)$  for each sample
2. Sort the sample indices  $(m_1, \dots, m_\eta)$  in descending order of  $\mathcal{L}(h_{\theta_i}(\mathbf{x}_n), y_n)$
3. Compute  $\delta_i$  from  $\delta_G$  for the  $i$ -th model using (6)
4. Define  $\eta_{\delta_i} = \lfloor \delta_i \eta \rfloor$
5. Minimize  $\frac{1}{\eta_{\delta_i}} \sum_{j=1}^{\eta_{\delta_i}} \mathcal{L}(h_{\theta_i}(\mathbf{x}_{m_j}), y_{m_j})$

**end for**

---

to unstable gradients and disrupting training. This phenomenon is observed empirically in our experiments, especially in early training stages.

When  $\delta_G$  approaches 1, the worst-case assumes a less pronounced divergence between train-test distributions. If  $\delta_G$  were to be set to 1, all samples would be selected for backpropagation, implying that  $w_n = 1$  for any  $n$  in (4). Consequently, the DRO loss components of all ensemble members would reduce to the ERM loss in (1), and CreDRO training would align with the standard ensemble. In this work,  $\delta_G$  is set to 0.5 by default to reflect a balanced degree of the train-test divergence and assess how this value helps our model outperform the baselines. In addition, our ablation study in Section 4.3 shows that CreDRO’s performance is robust to the choice of hyperparameter  $\delta_G$ .

The batch-wise CreDRO training procedure is outlined in Algorithm 1. Here,  $\mathcal{L}(\cdot, \cdot)$  could be any suitable loss, as long as it enables neural networks to produce probabilistic predictions, such as the cross-entropy (CE) loss or focal loss [Lin et al., 2017]. In this work, we adopt the widely used CE loss to ensure fair and consistent comparison with existing baselines.

**Distinctions from the CreDE baseline.** The method most closely related to our work is the recent credal deep ensemble (CreDE) approach [Wang et al., 2024], which also incorporates distributionally robust optimization (DRO) principles during training. However, several key distinctions set CreDRO apart. ① *Architecturally*, CreDE requires doubling the number of output neurons in the final layer in order to predict lower and upper probability bounds for each class. In contrast, CreDRO builds upon standard neural network architectures and requires *no architectural modifications*, thereby reducing model complexity and improving compatibility with existing training paradigms (see Table 3).

② Regarding individual ensemble members, CreDE uses the DRO loss (4) to train the lower probability bound and the ERM loss (1) for the upper bound. In contrast, our approach applies DRO to train a classical NN, representing a relaxed form of the i.i.d. training assumption. Furthermore, since CreDE’s upper and lower probability vectors are not normalized, it is restricted to one-hot label data when employing the CE loss [Wang et al., 2024], whereas CreDRO *does not suffer from this limitation*. ③ Regarding ensembling, CreDE uses a single fixed DRO hyperparameter, implicitly assuming the same train-test distribution divergence for all ensemble members. Consequently, disagreement among ensemble members arises mainly from random initialization. In contrast, CreDRO assigns *a range of* DRO hyperparameters to individual models, encouraging diverse probabilistic predictions that reflect varying relaxations of the i.i.d. assumption during training.

### 3.2 Credal prediction and uncertainty quantification

**Generating prediction.** For  $C$ -class classification problem, CreDRO transforms individual softmax probabilities  $\{\mathbf{p}_i\}_{i=1}^M$  into class-wise probability intervals as follows:

$$\bar{p}_k = \max_{i=1, \dots, M} p_{i,k} \quad \underline{p}_k = \min_{i=1, \dots, M} p_{i,k}, \quad (7)$$

where  $\bar{p}_k$  and  $\underline{p}_k$  denote the upper and lower probability interval bounds for the  $k$ -th class, and  $p_{i,k}$  is the  $k$ -th element of the given  $\mathbf{p}_i$ . These intervals induce a non-empty box credal set  $\mathcal{K}_B$  as follows [De Campos et al., 1994]:

$$\mathcal{K}_B = \left\{ \mathbf{p} \mid p_k \in [\underline{p}_k, \bar{p}_k] \text{ for } k=1, \dots, C \text{ and } \sum_{k=1}^C p_k = 1 \right\}. \quad (8)$$

$\mathcal{K}_B$  ensures a convex set of probability vectors, with each class probability value constrained to the specified interval.

There exists an alternative way to construct credal sets by taking the convex hull of a collection of probability vectors, denoted  $\mathcal{K}_C$ , as follows:

$$\mathcal{K}_C = \left\{ \sum_{i=1}^M \pi_i \mathbf{p}_i \mid \pi_i \geq 0, \sum_{i=1}^M \pi_i = 1 \right\}. \quad (9)$$

$\mathcal{K}_C$  is contained in the box credal set  $\mathcal{K}_B$ , i.e.,  $\mathcal{K}_C \subseteq \mathcal{K}_B$ , since the convex hull is the smallest convex set containing the given collection of probability vectors. Nonetheless, for binary classification,  $\mathcal{K}_C = \mathcal{K}_B$  as both are reduced to the same probability interval. From a computational perspective, however,  $\mathcal{K}_B$  enables more efficient computation of EU, as discussed in Appendix E.1. Accordingly, we adopt the box credal set  $\mathcal{K}_B$  in (8). Furthermore, the ablation study in Section 4.4 demonstrates that  $\mathcal{K}_B$  consistently outperforms  $\mathcal{K}_C$  across several OOD detection benchmarks.

**Uncertainty quantification.** We quantify EU of our credal prediction  $\mathcal{K}_B$  by computing the difference between upper and lower Shannon entropy [Abellán et al., 2006], written as  $\overline{H}(\mathcal{K}_B) - \underline{H}(\mathcal{K}_B)$ . Computing  $\overline{H}(\mathcal{K}_B)$  for CreDRO requires optimizing the following:

$$\begin{aligned} & \text{maximize} \sum_{k=1}^C -p_k \log p_k \\ & \text{s.t. } \sum_{k=1}^C p_k = 1 \text{ and } p_k \in [\underline{p}_k, \bar{p}_k] \text{ for } k=1, \dots, C \end{aligned}, \quad (10)$$

which searches for  $\mathbf{p}$  within  $\mathcal{K}_B$  to maximizes the entropy; computing  $\underline{H}(\mathcal{K}_B)$  requires minimization instead. Both problems can be efficiently solved using the SciPy tool [Virtanen et al., 2020], and incur only marginal computational overhead [Wang et al., 2024, 2025b]. Note that uncertainty quantification for credal sets remains an active research area; we consider alternative measures in the extended literature review (Appendix A).

## 4 Experimental validation

### 4.1 Comparison with SOTA credal classifiers and DE

Since groundtruth EU does not exist, *OOD detection* is commonly used as a practical benchmark for evaluate the quality of EU quantification, where stronger OOD detection performance indicates more informative uncertainty quantified [Wang et al., 2024, Löhr et al., 2025]. In this setting, OOD detection is formulated as a binary classification problem, with in-distribution (ID) and OOD

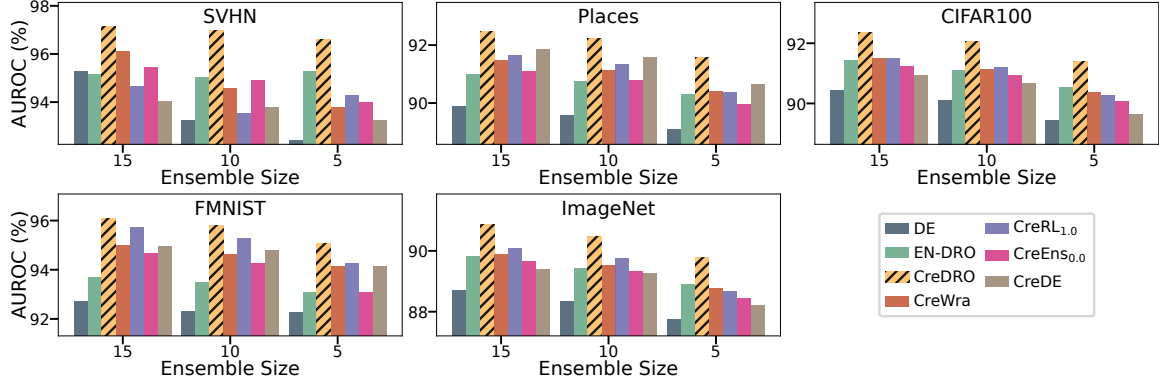


**Figure 2:** AUROC (%) for OOD detection using EU, across methods and ensemble sizes.

samples assigned to classes 0 and 1, respectively. The model’s uncertainty estimate is then used as the prediction score, and the performance is evaluated via the area under the receiver operating characteristic curve (AUROC).

**Setup.** We benchmark our CreDRO against several SOTA credal classifiers considered in a recent study [Löhr et al., 2025]: credal Bayesian deep learning (CreBNN) [Caprio et al., 2024], credal deep ensembles (CreDE) [Wang et al., 2024], the credal wrapper (CreWra) [Wang et al., 2025b], credal ensembling (CreEns) [Nguyen et al., 2025], and credal predictions based on relative likelihood (CreRL) [Löhr et al., 2025]. We also include two strong ensemble baselines: a standard deep ensemble (DE), and EN-DRO—an ensemble *trained with our DRO framework* in Algorithm 1 but *without generating credal predictions*. The experiment uses CIFAR10 [Krizhevsky et al., 2009] as the ID dataset, against several OOD datasets including SVHN [Hendrycks et al., 2021], Places365 [Zhou et al., 2018], CIFAR100 [Krizhevsky, 2012], FMNIST [Xiao et al., 2017], and ImageNet [Deng et al., 2009]. For a fair comparison, we follow the setup of Löhr et al. [2025] and continue training an ensemble ( $M=20$ ,  $\delta_G=0.5$ ) of ResNet18 models [He et al., 2016] on the CIFAR10 training data using our CreDRO method. The performance of CreRL and CreEns depends on a hyperparameter  $\alpha$ , and we report their best results. The CreDE training hyperparameter is set to 0.5, as recommended by Wang et al. [2024]. Additional experimental details are provided in Appendix B.1.

To compute EU estimates, we apply the upper and lower entropy differences across all credal classifiers. For individual softmax probabilities, i.e.,  $\{\mathbf{p}_i\}_{i=1}^M$ , of classical ensembles (DE & EN-DRO), we follow equation (5). **Results.** Table 1 reports the OOD detection scores across all methods. Our proposed CreDRO consistently performs the best, indicating its effective representation of EU.

The principled derivation of a single representative probability vector from credal sets remains an open problem [Löhr et al., 2025] and is outside the scope of this work. Nevertheless, for completeness, we show that simply using the averaged probability vector  $\tilde{\mathbf{p}} \in \mathcal{K}_B$  produced by CreDRO (which yields the same prediction as DRO) outperforms classical DE, achieving higher accuracy and lower expected calibration error (ECE) [Guo et al., 2017] on the CIFAR10 test set, as shown in Table 2. Note that ECE is also defined for single-probability predictions; a principled extension of ECE to credal sets requires further investigation [Wang et al., 2024, Chau et al., 2025b]. In addition, we report the test accuracy of each ensemble member for credal classifiers in Table 7 in the Appendix. The results show that the relaxation of the i.i.d. assumption during training also improves the test accuracy of the individual members of CreDRO.

**Table 1:** AUROC score (%) for OOD detection based on EU using CIFAR10 as ID dataset. Best scores are bold. Results are averaged over 3 runs.

	SVHN	Places	CIFAR100	FMNIST	ImageNet
DE	94.8 $\pm$ 0.3	90.0 $\pm$ 0.2	90.6 $\pm$ 0.0	92.9 $\pm$ 0.3	88.9 $\pm$ 0.1
<b>EN-DRO</b>	95.7 $\pm$ 0.0	91.1 $\pm$ 0.1	91.6 $\pm$ 0.1	94.0 $\pm$ 0.1	90.0 $\pm$ 0.1
<b>CreDRO</b>	<b>97.4</b> $\pm$ 0.1	<b>92.7</b> $\pm$ 0.1	<b>92.5</b> $\pm$ 0.1	<b>96.4</b> $\pm$ 0.0	<b>91.1</b> $\pm$ 0.1
CreWra	95.7 $\pm$ 0.3	91.6 $\pm$ 0.1	91.6 $\pm$ 0.0	95.2 $\pm$ 0.0	89.0 $\pm$ 0.1
CreRL <sub>1.0</sub>	94.8 $\pm$ 0.3	91.8 $\pm$ 0.2	91.6 $\pm$ 0.1	95.7 $\pm$ 0.2	88.9 $\pm$ 0.2
CreEns <sub>0.0</sub>	95.5 $\pm$ 0.1	91.3 $\pm$ 0.0	91.4 $\pm$ 0.1	94.9 $\pm$ 0.1	88.8 $\pm$ 0.0
CreDE	94.3 $\pm$ 0.3	91.8 $\pm$ 0.0	91.2 $\pm$ 0.0	95.1 $\pm$ 0.2	88.4 $\pm$ 0.1
CreBNN	90.7 $\pm$ 0.6	88.5 $\pm$ 0.2	88.0 $\pm$ 0.2	93.5 $\pm$ 0.2	85.9 $\pm$ 0.2

**Table 2:** Test accuracy and ECE comparison using the averaged probability vector as the single prediction. Best scores are bold.

	Test Accuracy	ECE
DE	0.9569 $\pm$ 0.0004	0.0051 $\pm$ 0.0004
<b>CreDRO</b>	<b>0.9637</b> $\pm$ 0.0004	<b>0.0038</b> $\pm$ 0.0008

To assess training complexity, we report the training runtime (in seconds) of credal classifiers trained on CIFAR10 with  $M = 5$ , measured on a single Nvidia A100-SXM4-40GB GPU. We also measure the inference time and UQ runtime (in seconds) on the CIFAR10 test set (1000 samples) using the same device. The results in Table 3 show that CreDRO achieves comparable performance on these metrics. Specifically, CreDRO is lighter than CreDE in terms of training and inference, since the latter has double-sized output neurons. The higher training complexity compared to classical ensemble training (CreWra & CreEns) arises because CreDRO orders the loss of individual samples within each batch (see Algorithm 1), introducing additional computation. For UQ runtime, CreEns is the heaviest, mainly because it deploys a convex-hull credal set as representation (see Appendix E.1 for further analysis). Appendix E.2 provides additional analysis of UQ runtime when employing box credal sets.

**Table 3:** Training and inference (including UQ) time comparison in seconds for credal classifiers on the CIFAR10 dataset. Mean with standard deviation over 3 runs.

	Training Time	Inference Time	UQ Runtime
CreDRO	6567.93 $\pm$ 35.78	1.89 $\pm$ 0.02	116.37 $\pm$ 0.30
CreEns <sub>0.0</sub>	6259.74 $\pm$ 15.01	2.07 $\pm$ 0.02	308.00 $\pm$ 7.93
CreWra	6259.74 $\pm$ 15.01	1.91 $\pm$ 0.02	123.83 $\pm$ 0.24
CreRL <sub>1.0</sub>	6679.69 $\pm$ 46.57	1.90 $\pm$ 0.02	133.31 $\pm$ 1.04
CreDE	6760.24 $\pm$ 52.81	2.03 $\pm$ 0.02	165.20 $\pm$ 0.96

## 4.2 Ablation study on ensemble size

**Setup.** This experiment further evaluates our CreDRO under different ensemble sizes, i.e.,  $M \in \{5, 10, 15\}$ , on the OOD detection benchmarks as in Section 4.1. All other experimental settings

remain unchanged.

**Results.** Figure 2 shows that CreDRO consistently outperforms all baselines, verifying its high-quality EU representation. In addition, the performance improves with larger ensemble sizes. Detailed scores appear in Table 8 in the Appendix. Furthermore, Figure 3 shows kernel density estimates [Silverman, 2018] of EU for both ID and OOD samples. CreDRO yields notably higher EU values for OOD samples than for ID ones, qualitatively verifying its reliable EU estimation. Similar positive results are observed in kernel density plots for other ensemble sizes in Figure 8 and Figure 9 in the Appendix.

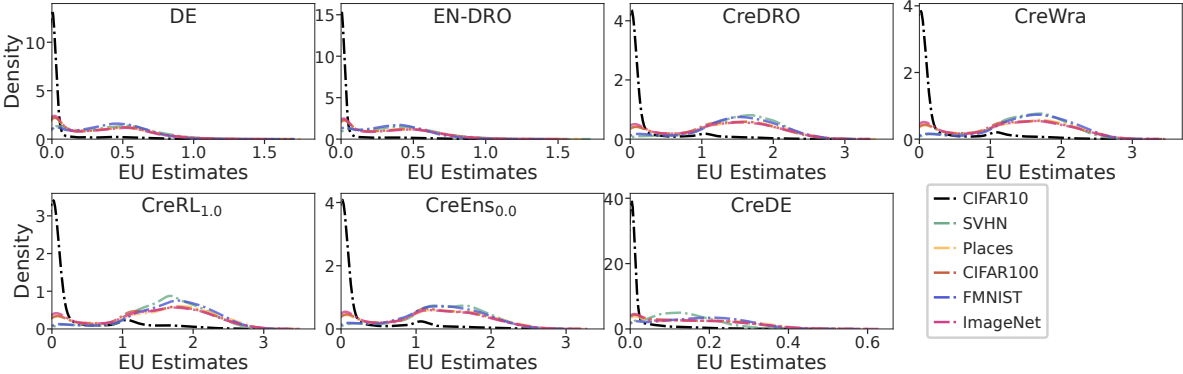


**Figure 3:** Kernel density plots of EU estimates on ID and OOD data from distinct methods. (ensemble size:  $M = 5$ ; first-run results)

### 4.3 Ablation study on training hyperparameter $\delta_G$

**Setup.** In the main experiment, we set  $\delta_G$  to 0.5 by default to reflect a balanced assessment of train-test divergence and to evaluate how this value helps our model outperform the baselines. This experiment conducts an ablation study on different values of the hyperparameter  $\delta_G$  in CreDRO training, i.e.,  $\delta_G \in \{0.5, 0.6, 0.7, 0.8, 0.9\}$ , and compare their OOD detection performance on benchmarks CIFAR10 vs SVHN, Places365, CIFAR100, FMNIST, and ImageNet. We use the setting  $M = 5$  and keep all other experimental configurations unchanged, as given in Section 4.1.

**Table 4:** AUROC score (%) of CreDRO trained with different values of  $\delta_G$  for OOD detection, using CIFAR10 as the ID dataset.

	SVHN	Places	CIFAR100	FMNIST	ImageNet
$\delta_G = 0.5$	96.6 $\pm$ 0.8	91.6 $\pm$ 0.1	91.4 $\pm$ 0.1	95.1 $\pm$ 0.1	89.8 $\pm$ 0.3
$\delta_G = 0.6$	96.2 $\pm$ 0.0	91.7 $\pm$ 0.0	91.3 $\pm$ 0.1	95.1 $\pm$ 0.3	89.8 $\pm$ 0.4
$\delta_G = 0.7$	95.8 $\pm$ 0.3	91.5 $\pm$ 0.1	91.2 $\pm$ 0.0	94.9 $\pm$ 0.0	89.6 $\pm$ 0.3
$\delta_G = 0.8$	96.3 $\pm$ 0.4	91.6 $\pm$ 0.0	91.3 $\pm$ 0.2	95.1 $\pm$ 0.1	89.8 $\pm$ 0.2
$\delta_G = 0.9$	96.1 $\pm$ 0.4	91.6 $\pm$ 0.0	91.4 $\pm$ 0.1	95.1 $\pm$ 0.3	89.8 $\pm$ 0.2

**Results.** Table 4 shows that CreDRO’s performance is stable across different choices of  $\delta_G$ . This is because  $\delta_G$  reflects only a single subjective belief of the model trainer about the worst-case training–test distribution divergence. In contrast, CreDRO incorporates multiple sensitivity levels

to potential distributional shifts through (6), which mitigates the effect of choosing a particular  $\delta_G$ . Additional empirical analysis is provided in Appendix D.

#### 4.4 Ablation study on credal set constructions

**Setup.** Building on our main experiment on OOD detection benchmarks in Section 4.1, we evaluate CreDRO under different credal-set construction methods, i.e.,  $\mathcal{K}_C$  in (9) and  $\mathcal{K}_B$  in (8). We vary the ensemble sizes, i.e.,  $M \in \{5, 10, 15, 20\}$ , while keeping all other experimental settings the same.

**Results.** Table 5 shows that using  $\mathcal{K}_B$  consistently outperforms  $\mathcal{K}_C$  across all applied OOD detection benchmarks. This could be explained by the fact that OOD detection depends on the relative magnitude of EU estimates between in-distribution (ID) and OOD samples. Since  $\mathcal{K}_C \subseteq \mathcal{K}_B$ , using  $\mathcal{K}_B$  tends to produce larger EU estimates for OOD samples, while the difference in estimates for ID samples is generally small. Therefore, the larger difference between EU estimates on OOD and ID samples produced by  $\mathcal{K}_B$  leads to a better OOD detection score.

**Table 5:** AUROC score (%) for OOD detection based on EU using CIFAR10 as the ID dataset, varying with different ensemble sizes. The best performance is highlighted in bold.

		SVHN	Places	CIFAR100	FMNIST	ImageNet
$M=5$	$\mathcal{K}_B$	<b>96.6</b> $\pm 0.8$	<b>91.6</b> $\pm 0.1$	<b>91.4</b> $\pm 0.1$	<b>95.1</b> $\pm 0.1$	<b>89.8</b> $\pm 0.3$
	$\mathcal{K}_C$	96.0 $\pm 0.9$	91.0 $\pm 0.1$	91.0 $\pm 0.1$	94.1 $\pm 0.1$	89.3 $\pm 0.3$
$M=10$	$\mathcal{K}_B$	<b>97.0</b> $\pm 0.1$	<b>92.2</b> $\pm 0.1$	<b>92.1</b> $\pm 0.0$	<b>95.8</b> $\pm 0.1$	<b>90.5</b> $\pm 0.1$
	$\mathcal{K}_C$	96.6 $\pm 0.1$	91.9 $\pm 0.1$	91.8 $\pm 0.0$	95.2 $\pm 0.2$	90.2 $\pm 0.1$
$M=15$	$\mathcal{K}_B$	<b>97.1</b> $\pm 0.3$	<b>92.5</b> $\pm 0.1$	<b>92.4</b> $\pm 0.1$	<b>96.1</b> $\pm 0.1$	<b>90.9</b> $\pm 0.2$
	$\mathcal{K}_C$	96.8 $\pm 0.4$	92.2 $\pm 0.1$	92.1 $\pm 0.1$	95.6 $\pm 0.1$	90.6 $\pm 0.2$
$M=20$	$\mathcal{K}_B$	<b>97.4</b> $\pm 0.1$	<b>92.7</b> $\pm 0.1$	<b>92.5</b> $\pm 0.1$	<b>96.4</b> $\pm 0.0$	<b>91.1</b> $\pm 0.1$
	$\mathcal{K}_C$	97.2 $\pm 0.1$	92.4 $\pm 0.1$	92.3 $\pm 0.1$	96.0 $\pm 0.1$	90.8 $\pm 0.2$

#### 4.5 Evaluation on corrupted data

**Setup.** This experiment uses OOD detection benchmarks on CIFAR10 vs CIFAR10-C [Hendrycks and Dietterich, 2019] and CIFAR100 vs CIFAR100-C [Hendrycks and Dietterich, 2019]. The CIFAR10-C and CIFAR100-C datasets apply 15 types of corruptions to the CIFAR10 and CIFAR100 original test samples, respectively, with 5 severity levels for each corruption type. These benchmarks allow us to further assess the UQ performance of CreDRO under data distribution shifts.

We mainly compare CreDRO with baselines that employ the DRO concept during training, namely EN-DRO and CreDE. To broaden the range of experimental settings, we conduct the CIFAR10 vs CIFAR10-C experiment using a pre-trained ResNet50, which is then fine-tuned on the CIFAR10 training set for all methods. The input images are resized to a shape of (224, 224, 3). For experiments involving CIFAR100, all methods are implemented on a wide residual network (WRN-28-4) backbone [Zagoruyko and Komodakis, 2016] and trained from scratch. Full implementation details are provided in Appendix B.2.

**Results.** Figure 4 shows the OOD detection comparison on CIFAR10 vs CIFAR10-C and CIFAR100 vs CIFAR100-C under increasing corruption intensities. The result demonstrates that our CreDRO significantly and consistently enhances EU estimation over baselines, as reflected by improved OOD detection performance across diverse dataset pairs and backbone architectures.

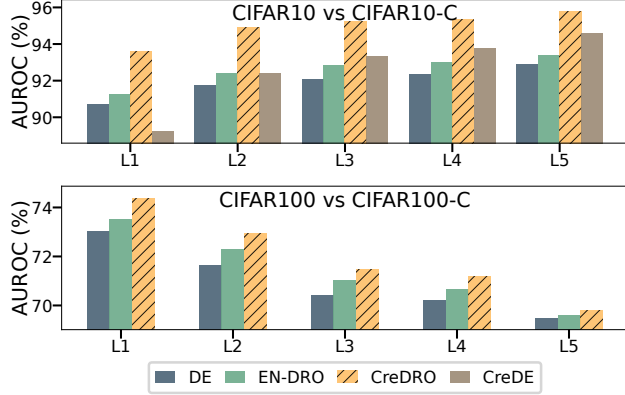


**Figure 4:** OOD detection score comparison across increasing levels of corruption. Results are averaged from 15 runs.

Note that the results of CreDE on CIFAR100 vs CIFAR100-C are missing because its generated probability intervals are too tight (see Figure 7 in the Appendix), making the optimization in (10) for calculating EU considerably difficult. For CIFAR100 vs CIFAR100-C, we did not observe a monotonic improvement in OOD detection as corruption intensity increased. This may be partly because corruption levels are defined from a human semantic perspective. Additionally, there is no consensus that detection performance should theoretically increase monotonically with increased corruption level.

#### 4.6 Selective classification in medical settings

**Setup.** In addition to OOD detection, *selective classification* is an alternative practical task for EU evaluation [Chau et al., 2025a]. In this task, the accuracy–rejection (AR) curve characterizes predictive accuracy as a function of the rejection rate. Specifically, when processing a batch of instances, samples with higher EU estimates are first rejected, and accuracy is computed on the remaining test data. With reliable uncertainty estimates, the AR curve exhibits a monotonic increasing trend [Hühn and Hüllermeier, 2008, Hüllermeier et al., 2022]. Besides, the area under the curve (AUC) is adopted for numerical comparison [Jaeger et al., 2023], where higher values indicate better performance.

This evaluation focuses on a real-world and large-scale binary histopathology image classification task on the Camelyon17 dataset [Bandi et al., 2018]. This setting conveys a strong and realistic domain-shift scenario [Mehrtens et al., 2023], where test samples are collected from different clinics and scanned using devices that differ from those used during training. Specifically, the data from centers 0, 1, and 3, which use 3DHistech scanners, make up the ID training and validation set. The test set consists of images from centers 2 and 4, which use Philips and Hamamatsu scanners, respectively, as shown in Table 6 in the Appendix.

Our implementation follows the recipe from Mehrtens et al. [2023]. Specifically, we train ResNet34-based DE, CreDRO, and CreDE models and evaluate their EU quantification performance on distribution-shifted test data. The full experimental setup is detailed in Appendix B.3.

**Results.** The AR curves and their AUC values in Figure 5 (top) show that our CreDRO achieves the best performance under this realistic distribution shift, while CreDE’s EU estimates appear unreliable, as accuracy decreases with higher rejection rates.

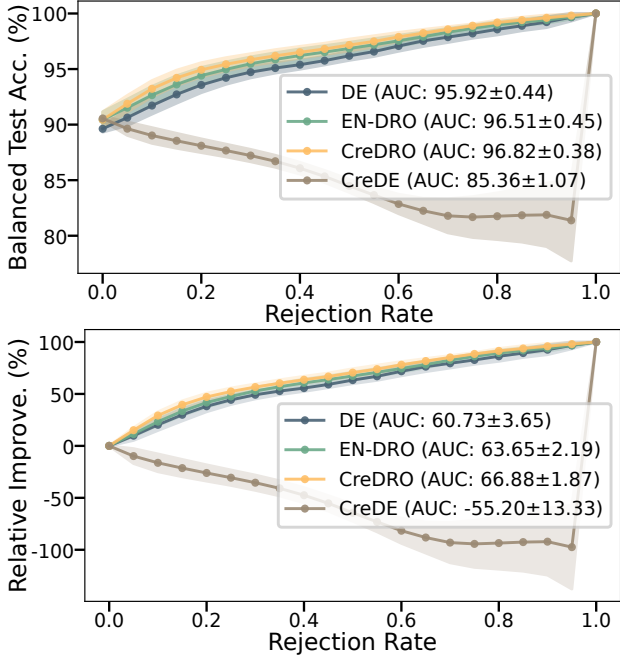


**Figure 5:** AR (top) and normalized AR (bottom) curves, along with the average AUC values. Note that the accuracy is set to 100% when the rejection rate reaches 1.0.

To decouple selective performance from the model’s base classification accuracy, we further report normalized AR curves, where accuracy gains are measured relative to the test accuracy without rejection. Specifically, let  $A(r)$  denote the accuracy at rejection rate  $r$ ; we define the relative accuracy improvement as  $\frac{A(r)-A(0)}{100\%-A(0)}$ . The result in Figure 5 (bottom) further supports the strong performance of CreDRO. Additionally, we present EU estimates for correctly and incorrectly classified samples in Figure 10 in the Appendix, showing CreDRO produces noticeably higher EU values for incorrectly-classified instances, confirming its reliable EU estimation.

## 5 Conclusion and future work

**Conclusion.** In this paper, we propose a novel approach for quantifying epistemic uncertainty, termed CreDRO. CreDRO learns an ensemble of plausible models via distributionally robust optimization by varying a weight hyperparameter to simulate different levels of potential train–test distribution shift during training, corresponding to different degrees of relaxation of the i.i.d. assumption. Extensive empirical results show that ① CreDRO consistently outperforms SOTA credal classifiers and strong deep ensemble baselines on OOD detection benchmarks, and ② improves performance in selective classification in a medical setting.

**Limitation & future work.** In our current work, we adopt a flexible implementation of the DRO strategy for efficient batch-wise training; exploring alternative formulations within the broader DRO family may further improve performance or provide additional insights. In addition, investigating principled approaches to derive a single predictive probability from credal sets remains an important and interesting direction for future research. Finally, a rigorous theoretical analysis and empirical studies on extending our CreDRO to regression tasks (a possible road-map is provided in Appendix F) are also left for future work.

## Acknowledgement

This work has received funding from the European Union’s Horizon 2020 research and innovation program under grant agreement No. 964505 (E-pi).

## References

Joaquín Abellán and Serafín Moral. A non-specificity measure for convex sets of probability distributions. *International journal of uncertainty, fuzziness and knowledge-based systems*, 8(03):357–367, 2000.

Joaquín Abellán, George J Klir, and Serafín Moral. Disaggregated total uncertainty measure for credal sets. *International Journal of General Systems*, 35(1):29–44, 2006.

Thomas Augustin, Frank PA Coolen, Gert De Cooman, and Matthias CM Troffaes. *Introduction to imprecise probabilities*. John Wiley & Sons, 2014.

Peter Bandi, Oscar Geessink, Quirine Manson, Marcory Van Dijk, Maschenka Balkenhol, Meyke Hermsen, Babak Ehteshami Bejnordi, Byungjae Lee, Kyunghyun Paeng, Aoxiao Zhong, et al. From detection of individual metastases to classification of lymph node status at the patient level: the camelyon17 challenge. *IEEE transactions on medical imaging*, 38(2):550–560, 2018.

Aharon Ben-Tal, Dick Den Hertog, Anja De Waegenaere, Bertrand Melenberg, and Gijs Rennen. Robust solutions of optimization problems affected by uncertain probabilities. *Management Science*, 59(2):341–357, 2013.

Viktor Bengs, Eyke Hüllermeier, and Willem Waegeman. On second-order scoring rules for epistemic uncertainty quantification. In *Proceedings of the Fortieth International Conference on Machine Learning*, volume 202 of *Proceedings of Machine Learning Research*, pages 2078–2091. PMLR, 23–29 Jul 2023.

Charles Blundell, Julien Cornebise, Koray Kavukcuoglu, and Daan Wierstra. Weight uncertainty in neural network. In *Proceedings of the International Conference on Machine Learning*, pages 1613–1622. PMLR, 2015.

Michele Caprio, Souradeep Dutta, Kuk Jin Jang, Vivian Lin, Radoslav Ivanov, Oleg Sokolsky, and Insup Lee. Credal Bayesian deep learning. *Transactions on Machine Learning Research*, 2024. ISSN 2835-8856.

Bertrand Charpentier, Daniel Zügner, and Stephan Günnemann. Posterior network: Uncertainty estimation without OOD samples via density-based pseudo-counts. *Advances in neural information processing systems*, 33:1356–1367, 2020.

Siu Lun Chau, Michele Caprio, and Krikamol Muandet. Integral imprecise probability metrics. In *The Thirty-ninth Annual Conference on Neural Information Processing Systems*, 2025a.

Siu Lun Chau, Antonin Schrab, Arthur Gretton, Dino Sejdinovic, and Krikamol Muandet. Credal two-sample tests of epistemic uncertainty. In *International Conference on Artificial Intelligence and Statistics*, pages 127–135. PMLR, 2025b.

Giorgio Corani and Marco Zaffalon. Learning reliable classifiers from small or incomplete data sets: The naive credal classifier 2. *Journal of Machine Learning Research*, 9(4), 2008.

Giorgio Corani, Alessandro Antonucci, and Marco Zaffalon. Bayesian networks with imprecise probabilities: Theory and application to classification. *Data Mining: Foundations and Intelligent Paradigms: Volume 1: Clustering, Association and Classification*, pages 49–93, 2012.

Luis M. De Campos, Juan F. Huete, and Serafin Moral. Probability intervals: A tool for uncertain reasoning. *International Journal of Uncertainty, Fuzziness and Knowledge-Based Systems*, 02: 167–196, June 1994. ISSN 0218-4885, 1793-6411.

Jia Deng, Wei Dong, Richard Socher, Li-Jia Li, Kai Li, and Li Fei-Fei. Imagenet: A large-scale hierarchical image database. In *2009 IEEE conference on computer vision and pattern recognition*, pages 248–255. Ieee, 2009.

Didier Dubois, Henri Prade, and Philippe Smets. Representing partial ignorance. *IEEE Transactions on Systems, Man, and Cybernetics-Part A: Systems and Humans*, 26(3):361–377, 2002.

John C Duchi, Peter W Glynn, and Hongseok Namkoong. Statistics of robust optimization: A generalized empirical likelihood approach. *Mathematics of Operations Research*, 46(3):946–969, 2021.

Nikita Durasov, Timur Bagautdinov, Pierre Baque, and Pascal Fua. Maskensembles for uncertainty estimation. In *Proceedings of the IEEE/CVF Conference on Computer Vision and Pattern Recognition*, pages 13539–13548, 2021.

Yarin Gal and Zoubin Ghahramani. Dropout as a Bayesian approximation: Representing model uncertainty in deep learning. In *Proceedings of the International Conference on Machine Learning*, pages 1050–1059. PMLR, 2016.

Chuan Guo, Geoff Pleiss, Yu Sun, and Kilian Q Weinberger. On calibration of modern neural networks. In *International conference on machine learning*, pages 1321–1330. PMLR, 2017.

Kaiming He, Xiangyu Zhang, Shaoqing Ren, and Jian Sun. Deep residual learning for image recognition. In *Proceedings of the IEEE conference on computer vision and pattern recognition*, pages 770–778, 2016.

Dan Hendrycks and Thomas Dietterich. Benchmarking neural network robustness to common corruptions and perturbations. *Proceedings of the International Conference on Learning Representations*, 2019.

Dan Hendrycks, Kevin Zhao, Steven Basart, Jacob Steinhardt, and Dawn Song. Natural adversarial examples. In *Proceedings of the IEEE/CVF Conference on Computer Vision and Pattern Recognition*, pages 15262–15271, 2021.

Zeyi Huang, Haohan Wang, Dong Huang, Yong Jae Lee, and Eric P Xing. The two dimensions of worst-case training and their integrated effect for out-of-domain generalization. In *Proceedings of the IEEE/CVF Conference on Computer Vision and Pattern Recognition*, pages 9631–9641, 2022.

Jens Christian Hühn and Eyke Hüllermeier. Fr3: A fuzzy rule learner for inducing reliable classifiers. *IEEE Transactions on Fuzzy Systems*, 17(1):138–149, 2008.

Eyke Hüllermeier and Willem Waegeman. Aleatoric and epistemic uncertainty in machine learning: An introduction to concepts and methods. *Machine Learning*, 110(3):457–506, 2021.

Eyke Hüllermeier, Sébastien Destercke, and Mohammad Hossein Shaker. Quantification of credal uncertainty in machine learning: A critical analysis and empirical comparison. In *Proceedings of the Uncertainty in Artificial Intelligence*, pages 548–557. PMLR, 2022.

Paul F Jaeger, Carsten Tim Lüth, Lukas Klein, and Till J. Bungert. A call to reflect on evaluation practices for failure detection in image classification. In *The Eleventh International Conference on Learning Representations*, 2023.

Mira Juergens, Nis Meinert, Viktor Bengs, Eyke Hüllermeier, and Willem Waegeman. Is epistemic uncertainty faithfully represented by evidential deep learning methods? In *Forty-first International Conference on Machine Learning*, 2024.

Alex Krizhevsky. Learning multiple layers of features from tiny images. *University of Toronto*, 05 2012.

Alex Krizhevsky, Vinod Nair, and Geoffrey Hinton. CIFAR-10 (Canadian Institute For Advanced Research). Technical report, CIFAR, 2009.

David Krueger, Chin-Wei Huang, Riashat Islam, Ryan Turner, Alexandre Lacoste, and Aaron Courville. Bayesian hypernetworks. *ArXiv Preprint ArXiv:1710.04759*, 2017.

Preethi Lahoti, Alex Beutel, Jilin Chen, Kang Lee, Flavien Prost, Nithum Thain, Xuezhi Wang, and Ed Chi. Fairness without demographics through adversarially reweighted learning. *Advances in neural information processing systems*, 33:728–740, 2020.

Balaji Lakshminarayanan, Alexander Pritzel, and Charles Blundell. Simple and scalable predictive uncertainty estimation using deep ensembles. *Advances in Neural Information Processing Systems*, 30, 2017.

Olivier Laurent, Adrien Lafage, Enzo Tartaglione, Geoffrey Daniel, Jean-marc Martinez, Andrei Bursuc, and Gianni Franchi. Packed ensembles for efficient uncertainty estimation. In *The Eleventh International Conference on Learning Representations*, 2022.

Nils Lehmann, Jakob Gawlikowski, Adam J. Stewart, Vytautas Jancauskas, Stefan Depeweg, Eric Nalisnick, and Nina Maria Gottschling. Lightning uq box: A comprehensive framework for uncertainty quantification in deep learning, 2024. URL <https://arxiv.org/abs/2410.03390>.

Isaac Levi. *The enterprise of knowledge: An essay on knowledge, credal probability, and chance*. MIT press, 1980.

Tsung-Yi Lin, Priya Goyal, Ross Girshick, Kaiming He, and Piotr Dollár. Focal loss for dense object detection. In *Proceedings of the IEEE international conference on computer vision*, pages 2980–2988, 2017.

Jessie Liu, Blanca Gallego, and Sebastiano Barbieri. Incorporating uncertainty in learning to defer algorithms for safe computer-aided diagnosis. *Scientific reports*, 12(1):1762, 2022.

Timo Löhr, Paul Hofman, Felix Mohr, and Eyke Hüllermeier. Credal prediction based on relative likelihood. In *The Thirty-ninth Annual Conference on Neural Information Processing Systems*, 2025.

Andrey Malinin and Mark Gales. Predictive uncertainty estimation via prior networks. *Advances in neural information processing systems*, 31, 2018.

Andrey Malinin and Mark Gales. Reverse kl-divergence training of prior networks: Improved uncertainty and adversarial robustness. *Advances in Neural Information Processing Systems*, 32, 2019.

Shireen Kudukkil Manchingal, Muhammad Mubashar, Kaizheng Wang, and Fabio Cuzzolin. A unified evaluation framework for epistemic predictions. In *International Conference on Artificial Intelligence and Statistics*, pages 2017–2025. PMLR, 2025a.

Shireen Kudukkil Manchingal, Muhammad Mubashar, Kaizheng Wang, Keivan Shariatmadar, and Fabio Cuzzolin. Random-set neural networks. In *The Thirteenth International Conference on Learning Representations*, 2025b.

Denis D Mauá, Fabio G Cozman, Diarmuid Conaty, and Cassio P Campos. Credal sum-product networks. In *Proceedings of the Tenth International Symposium on Imprecise Probability: Theories and Applications*, pages 205–216. PMLR, 2017.

Hendrik A Mehrtens, Alexander Kurz, Tabea-Clara Bucher, and Titus J Brinker. Benchmarking common uncertainty estimation methods with histopathological images under domain shift and label noise. *Medical Image Analysis*, 89:102914, 2023.

Aryan Mobiny, Pengyu Yuan, Supratik K Moulik, Naveen Garg, Carol C Wu, and Hien Van Nguyen. Dropconnect is effective in modeling uncertainty of Bayesian deep networks. *Scientific Reports*, 11(1):1–14, 2021.

Bálint Mucsányi, Michael Kirchhof, and Seong Joon Oh. Benchmarking uncertainty disentanglement: Specialized uncertainties for specialized tasks. *arXiv preprint arXiv:2402.19460*, 2024.

Jishnu Mukhoti, Andreas Kirsch, Joost van Amersfoort, Philip HS Torr, and Yarin Gal. Deep deterministic uncertainty: A new simple baseline. In *Proceedings of the IEEE/CVF Conference on Computer Vision and Pattern Recognition*, pages 24384–24394, 2023.

Junhyun Nam, Hyuntak Cha, Sungsoo Ahn, Jaeho Lee, and Jinwoo Shin. Learning from failure: De-biasing classifier from biased classifier. *Advances in Neural Information Processing Systems*, 33:20673–20684, 2020.

Vu-Linh Nguyen, Haifei Zhang, and Sébastien Destercke. Credal ensembling in multi-class classification. *Machine Learning*, 114(1):19, 2025. ISSN 1573-0565.

Yonatan Oren, Shiori Sagawa, Tatsunori B Hashimoto, and Percy Liang. Distributionally robust language modeling. *arXiv preprint arXiv:1909.02060*, 2019.

Shiori Sagawa, Pang Wei Koh, Tatsunori B Hashimoto, and Percy Liang. Distributionally robust neural networks for group shifts: On the importance of regularization for worst-case generalization. *arXiv preprint arXiv:1911.08731*, 2019.

Yusuf Sale, Michele Caprio, and Eyke Hüllermeier. Is the volume of a credal set a good measure for epistemic uncertainty? In *Uncertainty in Artificial Intelligence*, pages 1795–1804. PMLR, 2023.

Mohammad Hossein Shaker and Eyke Hüllermeier. Ensemble-based uncertainty quantification: Bayesian versus credal inference. In *Proceedings of 31st Workshop Computational Intelligence*, volume 25, page 63, 2021a.

Mohammad Hossein Shaker and Eyke Hüllermeier. Ensemble-based uncertainty quantification: Bayesian versus credal inference. In *Proceedings 31. workshop computational intelligence*, volume 25, page 63, 2021b.

Maohao Shen, Jongha Jon Ryu, Soumya Ghosh, Yuheng Bu, Prasanna Sattigeri, Subhro Das, and Gregory W. Wornell. Are uncertainty quantification capabilities of evidential deep learning a

mirage? In *The Thirty-eighth Annual Conference on Neural Information Processing Systems*, 2024.

Bernard W Silverman. *Density estimation for statistics and data analysis*. Routledge, 2018.

Ankit Singh, Siu Lun Chau, Soumaya Bouabid, and Krikamol Muandet. Domain generalisation via imprecise learning. In *Proceedings of the 41st International Conference on Machine Learning*, volume 235 of *Proceedings of Machine Learning Research*, pages 45544–45570. PMLR, 2024.

Laurens Sluijterman, Eric Cator, and Tom Heskes. Optimal training of mean variance estimation neural networks. *Neurocomputing*, 597:127929, September 2024. ISSN 0925-2312. doi: 10.1016/j.neucom.2024.127929. URL <http://dx.doi.org/10.1016/j.neucom.2024.127929>.

Rui Tuo and Wenjia Wang. Uncertainty quantification for Bayesian optimization. In Gustau Camps-Valls, Francisco J. R. Ruiz, and Isabel Valera, editors, *Proceedings of The 25th International Conference on Artificial Intelligence and Statistics*, volume 151 of *Proceedings of Machine Learning Research*, pages 2862–2884. PMLR, 28–30 Mar 2022.

Pauli Virtanen, Ralf Gommers, Travis E. Oliphant, et al. SciPy 1.0: Fundamental Algorithms for Scientific Computing in Python. *Nature Methods*, 17:261–272, 2020.

Kaizheng Wang, Fabio Cuzzolin, Shireen Kudukkil Manchingal, Keivan Shariatmadar, David Moens, and Hans Hallez. Credal deep ensembles for uncertainty quantification. In *The Thirty-eighth Annual Conference on Neural Information Processing Systems*, 2024.

Kaizheng Wang, Fabio Cuzzolin, David Moens, and Hans Hallez. Credal ensemble distillation for uncertainty quantification. *arXiv preprint arXiv:2511.13766*, 2025a.

Kaizheng Wang, Fabio Cuzzolin, Keivan Shariatmadar, David Moens, and Hans Hallez. Credal wrapper of model averaging for uncertainty estimation in classification. In *The Thirteenth International Conference on Learning Representations*, 2025b.

Kaizheng Wang, Keivan Shariatmadar, Shireen Kudukkil Manchingal, Fabio Cuzzolin, David Moens, and Hans Hallez. CreINNs: Credal-set interval neural networks for uncertainty estimation in classification tasks. *Neural Networks*, 185:107198, 2025c. ISSN 0893-6080.

Kaizheng Wang, Fabio Cuzzolin, Keivan Shariatmadar, David Moens, and Hans Hallez. A review of uncertainty representation and quantification in neural networks. *IEEE Transactions on Pattern Analysis and Machine Intelligence*, 48(3):2476–2495, 2026. doi: 10.1109/TPAMI.2025.3626645.

Yeming Wen, Dustin Tran, and Jimmy Ba. Batchensemble: an alternative approach to efficient ensemble and lifelong learning. *arXiv preprint arXiv:2002.06715*, 2020.

Han Xiao, Kashif Rasul, and Roland Vollgraf. Fashion-MNIST: a novel image dataset for benchmarking machine learning algorithms, 2017.

Marco Zaffalon. The naive credal classifier. *Journal of statistical planning and inference*, 105(1): 5–21, 2002.

Sergey Zagoruyko and Nikos Komodakis. Wide residual networks. *arXiv preprint arXiv:1605.07146*, 2016.

Bolei Zhou, Agata Lapedriza, Aditya Khosla, Aude Oliva, and Antonio Torralba. Places: A 10 million image database for scene recognition. *IEEE Transactions on Pattern Analysis and Machine Intelligence*, 40(6):1452–1464, 2018. doi: 10.1109/TPAMI.2017.2723009.

Dengyong Zhou, Sumit Basu, Yi Mao, and John Platt. Learning from the wisdom of crowds by minimax entropy. *Advances in Neural Information Processing Systems*, 25, 2012.

## A Extended related work

Credal sets have recently gained growing interest within the broader machine learning community for epistemic uncertainty (EU) quantification, even prior to their application in deep learning [Wang et al., 2024, Nguyen et al., 2025, Wang et al., 2025b, Löhr et al., 2025, Wang et al., 2025a, Manchingal et al., 2025a]. Relevant studies include [Zaffalon, 2002, Corani and Zaffalon, 2008, Corani et al., 2012, Mauá et al., 2017, Hüllermeier and Waegeman, 2021, Shaker and Hüllermeier, 2021a, Sale et al., 2023]. A key benefit of credal sets is their unification of set-based and distribution-based concepts into a single framework. This makes them a more natural way to represent epistemic uncertainty than modeling with individual probability distributions [Corani et al., 2012, Hüllermeier and Waegeman, 2021]. For instance, one can argue that sets better capture ignorance as a lack of knowledge [Dubois et al., 2002], since distributions inherently rely on extra assumptions beyond simply distinguishing between plausible and implausible candidates [Löhr et al., 2025]. For more motivations for working with credal sets for uncertainty quantification, please refer to Appendix A of Caprio et al. [2024].

In deep learning, a recent credal wrapper (CreWra) approach [Wang et al., 2025b] formulates credal set predictions from the multiple softmax predictions from members of a deep ensemble (DE) [Lakshminarayanan et al., 2017] trained with different random initializations. A credal ensembling (CreEns) [Nguyen et al., 2025] acts as an alternative post hoc extension to a classical ensemble that also enables discarding outlier probabilities, preventing credal sets from becoming too large. Credal predictions based on relative likelihood (CreRL) [Löhr et al., 2025] proposes a Tobias scheme to increase diversity in ensemble initialization and a selection process based on a predefined threshold ( $\alpha$  cut) to identify plausible members of an ensemble by their relative likelihood. Although these credal predictors improve EU estimation, they mainly focus on classification and capture EU stemming from ensemble disagreement due to random initializations. They fail to adequately reflect ignorance caused by potential shifts between training and testing distributions—a critical challenge in practical applications. Alternatively, a recent approach, credal deep ensemble (CreDE) (also used as a baseline in our comparison), directly trains neural networks to predict probability intervals by outputting a lower and an upper probability for each class [Wang et al., 2024]. Although also incorporating the distributionally robust optimization (DRO) concept in learning the lower probability bounds, the training scheme between CreDRO and CreDE is quite different, as we detailed in Section 3.1. In addition, our extensive experiments in Section 4 demonstrate that our CreDRO consistently outperforms CreDE. From the practical perspectives, these aforementioned methods present distinct constraints: CreDE requires modifying the model’s last layer; CreWra and CreEns operate solely as post-hoc processors; and CreRL relies on a maximum-likelihood estimator as a reference model and lacks a clear criterion for choosing  $\alpha$ . These limitations restrict broader applicability in practice.

Beyond these recent advancements, other credal methods exist: credal Bayesian deep learning (CreBNN) [Caprio et al., 2024], which we also employ as a baseline for comparison in Section 4. CreBNN represents weights and predictions as credal sets and has demonstrated robustness; however, the setting of credal set prior still relies on random initialization and its computational cost is comparable to that of Bayesian neural network ensembles, significantly limiting practical applicability. Additionally, Wang et al. [2025c] introduces credal-set interval neural networks, which construct credal sets from probability intervals derived from the deterministic interval outputs of interval neural networks. This approach offers a unique capability for uncertainty quantification (UQ) with interval input data and achieves EU quantification performance comparable to deep ensembles, particularly on smaller datasets, with greater efficiency. Nonetheless, its computational cost hinders

scalability. Since improving EU quality is one of our primary focuses, its comparable performance with deep ensembles, coupled with the scalability constraint, led us to exclude it from our baselines. Moreover, another approach generates credal predictions using belief functions defined by a random-set output [Manchingal et al., 2025b]. Training such a model requires a budgeting process to select the most relevant class and to convert the original one-hot labels into belief-function form. This deviates from our setting, e.g., learning is based on the given original data. Thus, we do not include it as a baseline.

Uncertainty quantification for credal sets remains an active area of research [Hüllermeier and Waegeman, 2021, Sale et al., 2023]. In classification problems, the notions of generalized entropy [Abellán et al., 2006] and the generalized Hartley (GH) measure [Abellán and Moral, 2000, Hüllermeier et al., 2022] have been introduced. However, practical application of the GH measure is often hindered by the computational complexity of solving constrained optimization problems over  $2^C$  subsets [Hüllermeier and Waegeman, 2021, Hüllermeier et al., 2022], which becomes especially challenging when the number of classes  $C$  is large (e.g.,  $C = 100$ ). Since intervals represent credal sets in the special binary case, [Hüllermeier et al., 2022] recently proposed using the width of the probability interval as an EU measure. Their results indicate that this measure offers improved theoretical properties and empirical performance compared to generalized entropy [Abellán et al., 2006] and the GH measure in the binary case. More recently, an imprecise probability metric framework proposes the maximum mean imprecision measure based on the total variance distance to quantify credal epistemic uncertainty [Chau et al., 2025a]. We include generalized entropy in multiclass classification primarily to enable fair comparison, as it is widely used among state-of-the-art credal classifiers.

## B Experiment details

This section details the experimental setup for our evaluation. The datasets are drawn from existing literature. *To support reproducibility, the core implementation code for running and analyzing the experiments will be released publicly upon publication under a license that allows free use for research.*

### B.1 Comparison with SOTA credal classifiers and DE baseline

In this experiment, we follow the experimental setup of Löhr et al. [Löhr et al., 2025]. The training procedures for the baselines, including CreBNN [Caprio et al., 2024], CreDE [Wang et al., 2024], CreWra [Wang et al., 2025b], CreEns [Nguyen et al., 2025], and CreRL [Löhr et al., 2025], are reproduced using the official GitHub repository <https://github.com/timoverse/credal-prediction-relative-likeness>. We then train CreDRO with the training hyperparameter set to  $\delta_G = 0.5$ , under the same settings to ensure a fair comparison.

Specifically, we use the PyTorch ResNet18 implementation and hyperparameters provided by <https://github.com/kuangliu/pytorch-cifar>. This model is optimized for CIFAR10 and is trained from scratch without any pretraining on ImageNet. The model is trained for 200 epochs with an initial learning rate of 0.1. We use SGD as the optimizer with a weight decay of 0.0005 and a batch size of 128. A cosine annealing learning rate scheduler is applied to gradually decay the learning rate during training. All experiments are conducted on a single Nvidia A100-SXM4-80GB GPU.

**Expected calibration error (ECE) evaluation.** Within the ECE framework, a single proba-

bilistic prediction is considered well calibrated if predictions made with a confidence of 80% are correct in roughly 80% of cases. To compute ECE, model predictions are partitioned into a fixed number  $G$  of confidence bins  $B_g$ , each covering an equal interval of confidence scores. The ECE metric is obtained by aggregating the weighted absolute differences between the empirical accuracy and the average confidence in each bin [Mehrtens et al., 2023]:

$$\sum_{g=1}^G \frac{|B_g|}{n} |\text{acc}(B_g) - \text{conf}(B_g)|, \quad (11)$$

where  $|B_g|$  denotes the number of samples assigned to the  $g$ -th bin, and  $n$  represents the total number of samples. Following common practice, we set the number of bins to the default value of  $G = 10$  in our experiments.

## B.2 Evaluation on corrupted data

To broaden the range of experimental settings, we conduct the CIFAR10 vs CIFAR10-C experiment using a pre-trained ResNet50, which is then fine-tuned on the CIFAR10 training set for all methods, in the framework of TensorFlow. The input images are resized to (224, 224, 3). For experiments involving CIFAR100, a wide residual network (WRN-28-4) [Zagoruyko and Komodakis, 2016] is used as the backbone and trained from scratch for all methods.

Regarding fine-tuning on the pre-trained ResNet50 using CIFAR10, standard data augmentation is applied uniformly across all methods to improve data quality and enhance training performance. The training batch size is set as 128. The standard data split is applied. The Adam optimizer is employed, with a learning rate scheduler set at 0.001 and reduced to 0.0001 during the final 5 training epochs. All models are trained using a single NVIDIA Tesla P100 SXM2 GPU for 20 epochs under different random seeds.

For scratch training on WRN-28-4 using CIFAR100, we use a learning rate schedule with linear warm-up followed by cosine annealing to improve training stability and performance, and train all methods for 200 epochs. Specifically, the learning rate is linearly increased from  $10^{-3}$  to 0.1 during the first 5 epochs and then decayed to  $10^{-6}$  using a cosine schedule over the remaining epochs. We use SGD with learning rate 0.1, momentum 0.9, and weight decay set to  $5 \times 10^{-6}$ . The other configurations, such as data split, batch size, data augmentation, and training hardware, remain unchanged.

## B.3 Selective classification in medical settings

Building on the work in [Mehrtens et al., 2023], this case study uses the Camelyon17 [Bandi et al., 2018] histopathological dataset for binary classification into Tumor, Non-Tumor. The dataset contains whole slide images (WSIs) of breast lymph node tissue with lesion-level annotations highlighting metastatic areas. Camelyon17 includes 50 WSIs collected from five medical centers in the Netherlands, captured using three different scanner types. An example WSI is shown in Figure 6.

To convey a strong domain shift scenario [Mehrtens et al., 2023], the dataset is split so that the test set only contains images from scanners not present in the in-distribution (ID) training data, introducing an additional technological variation. Specifically, WSIs from centers 0, 1, and 3, which use 3DHistech scanners, make up the ID training and validation set. The test set consists of images

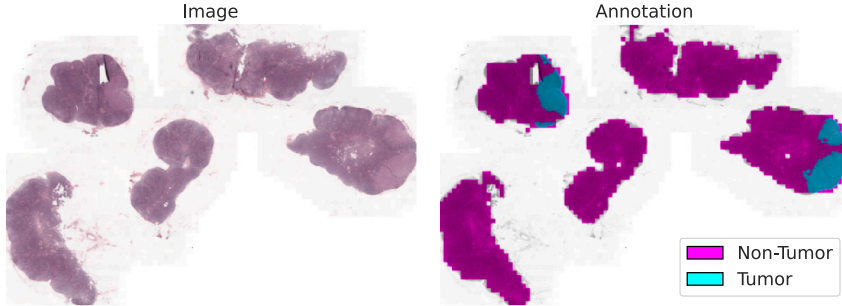


**Figure 6:** An example of the whole slide image (referring node 2 of patient 017 in the Camelyon17 dataset) with ground-truth annotations.

**Table 6:** Camelyon17 medical tile image instances data split applied in the experiment, where the input shape is (3, 224, 224).

	Train	Validation	Test
Clinic centers	0, 1, 3	0, 1, 3	2, 4
Scanner	3D Histech	3D Histech	Philips, Hamamatsu
# Instances	383406	110561	255968

from centers 2 and 4, which use Philips and Hamamatsu scanners, respectively. The detailed data split is summarized in Table 6.

For the training configurations, we follow the official GitHub repository <https://github.com/DB0-DKFZ/uncertainty-benchmark> to train the deep ensemble (DE) model ( $M = 5$ ), using the approach outlined in [Mehrtens et al. \[2023\]](#). We then adjust the training of CreDRO and CreDE by setting the training hyperparameter to 0.5, as suggested in the original work, to ensure a fair comparison. The neural network backbone is ResNet34, trained from scratch on a single NVIDIA Tesla P100 SXM2 GPU. All other settings, including data augmentation, optimizer, learning rate, and others, follow the default configurations of the repository. Considering mainly the computational cost, we conduct each experiment over 5 runs.

Note that, in the special case of binary classification, the credal set reduces to a single probability interval denoted as  $[\underline{p}, \bar{p}]$ . [Hüllermeier et al., 2022](#) have recently proposed using the width of this interval as an EU measure, i.e.,  $\bar{p} - \underline{p}$ , which shows better theoretical properties and empirical performance than generalized entropy [\[Abellán et al., 2006\]](#). For this reason, we adopt this measure in our experiments.

## C Additional experiment results

**Table 7:** Test accuracy of each ensemble member in credal classifiers on the CIFAR10 test set, providing insight into their individual performance. For CreDE, whose ensemble members directly predict probability intervals, we apply their intersection probability technique to obtain pointwise predictions [Wang et al., 2025b], following the setting of Löhr et al. [2025]. The results show that incorporating DRO during training also improves the test accuracy of the individual members of CreDRO.

Member Index	CreWra	<b>CreDRO</b>	CreEns	CreBNN	CreDE	CreRL <sub>1,0</sub>
1	0.942±0.001	0.954±0.001	0.955±0.000	0.875±0.004	0.941±0.000	0.943±0.001
2	0.944±0.001	0.953±0.002	0.954±0.000	0.877±0.005	0.943±0.000	0.934±0.001
3	0.944±0.001	0.953±0.001	0.952±0.001	0.867±0.015	0.944±0.001	0.934±0.002
4	0.943±0.002	0.954±0.003	0.952±0.000	0.881±0.003	0.942±0.001	0.936±0.001
5	0.943±0.001	0.953±0.000	0.952±0.001	0.872±0.004	0.942±0.001	0.935±0.002
6	0.943±0.000	0.954±0.001	0.952±0.000	0.869±0.006	0.942±0.002	0.934±0.002
7	0.941±0.001	0.954±0.001	0.952±0.001	0.877±0.001	0.943±0.001	0.936±0.001
8	0.942±0.001	0.955±0.000	0.951±0.001	0.880±0.006	0.943±0.002	0.935±0.001
9	0.943±0.001	0.953±0.001	0.951±0.000	0.879±0.005	0.944±0.001	0.936±0.002
10	0.943±0.000	0.954±0.001	0.953±0.000	0.873±0.007	0.943±0.003	0.936±0.001
11	0.942±0.001	0.954±0.002	0.953±0.001	0.882±0.004	0.943±0.000	0.936±0.001
12	0.943±0.000	0.953±0.003	0.953±0.000	0.879±0.003	0.942±0.000	0.934±0.002
13	0.943±0.000	0.955±0.001	0.953±0.001	0.874±0.000	0.943±0.002	0.937±0.002
14	0.945±0.000	0.954±0.001	0.952±0.001	0.872±0.006	0.941±0.001	0.934±0.002
15	0.942±0.002	0.952±0.001	0.948±0.000	0.856±0.019	0.942±0.001	0.933±0.002
16	0.942±0.000	0.953±0.002	0.941±0.000	0.870±0.002	0.942±0.001	0.936±0.002
17	0.942±0.001	0.955±0.000	0.930±0.001	0.854±0.035	0.942±0.002	0.935±0.001
18	0.944±0.001	0.954±0.001	0.921±0.001	0.872±0.007	0.943±0.002	0.934±0.001
19	0.943±0.001	0.954±0.001	0.906±0.002	0.873±0.001	0.942±0.001	0.936±0.001
20	0.942±0.001	0.956±0.001	0.872±0.002	0.860±0.012	0.942±0.001	0.935±0.002
Average	0.9428	<b>0.95385</b>	0.94265	0.8721	0.94245	0.93545

**Table 8:** AUROC score (%) for OOD detection based on EU using CIFAR10 as the ID dataset. The best performance is highlighted in bold. Results vary with different ensemble sizes, showing that CreDRO consistently outperforms all baselines, further confirming its high-quality EU representation.

	SVHN	Places	CIFAR100	FMNIST	ImageNet
Ensemble Number $M = 5$					
DE	92.4 $\pm$ 0.3	89.1 $\pm$ 0.2	89.4 $\pm$ 0.2	92.3 $\pm$ 0.2	87.7 $\pm$ 0.2
<b>EN-DRO</b>	95.3 $\pm$ 0.9	90.3 $\pm$ 0.1	90.5 $\pm$ 0.0	93.1 $\pm$ 0.2	88.9 $\pm$ 0.1
<b>CreDRO</b>	<b>96.6<math>\pm</math>0.8</b>	<b>91.6<math>\pm</math>0.1</b>	<b>91.4<math>\pm</math>0.1</b>	<b>95.1<math>\pm</math>0.1</b>	<b>89.8<math>\pm</math>0.3</b>
CreWra	93.8 $\pm$ 0.3	90.4 $\pm$ 0.2	90.4 $\pm$ 0.1	94.1 $\pm$ 0.2	88.8 $\pm$ 0.2
CreRL <sub>1.0</sub>	94.3 $\pm$ 0.3	90.4 $\pm$ 0.1	90.3 $\pm$ 0.1	94.3 $\pm$ 0.2	88.7 $\pm$ 0.1
CreEns <sub>0.0</sub>	94.0 $\pm$ 0.6	89.9 $\pm$ 0.1	90.1 $\pm$ 0.0	93.1 $\pm$ 0.1	88.5 $\pm$ 0.2
CreDE	93.2 $\pm$ 0.6	90.6 $\pm$ 0.2	89.6 $\pm$ 0.2	94.1 $\pm$ 0.3	88.2 $\pm$ 0.3
Ensemble Number $M = 10$					
DE	93.3 $\pm$ 0.5	89.6 $\pm$ 0.2	90.1 $\pm$ 0.1	92.3 $\pm$ 0.4	88.4 $\pm$ 0.1
<b>EN-DRO</b>	95.1 $\pm$ 0.1	90.8 $\pm$ 0.1	91.1 $\pm$ 0.0	93.5 $\pm$ 0.2	89.4 $\pm$ 0.1
<b>CreDRO</b>	<b>97.0<math>\pm</math>0.1</b>	<b>92.2<math>\pm</math>0.1</b>	<b>92.1<math>\pm</math>0.0</b>	<b>95.8<math>\pm</math>0.1</b>	<b>90.5<math>\pm</math>0.1</b>
CreWra	94.6 $\pm$ 0.3	91.1 $\pm$ 0.2	91.1 $\pm$ 0.1	94.6 $\pm$ 0.3	89.5 $\pm$ 0.1
CreRL <sub>1.0</sub>	93.6 $\pm$ 0.3	91.3 $\pm$ 0.2	91.2 $\pm$ 0.1	95.3 $\pm$ 0.2	89.8 $\pm$ 0.0
CreEns <sub>0.0</sub>	94.9 $\pm$ 0.7	90.8 $\pm$ 0.1	90.9 $\pm$ 0.1	94.3 $\pm$ 0.2	89.3 $\pm$ 0.1
CreDE	93.8 $\pm$ 0.3	91.6 $\pm$ 0.2	90.7 $\pm$ 0.1	94.8 $\pm$ 0.2	89.3 $\pm$ 0.1
Ensemble Number $M = 15$					
DE	95.3 $\pm$ 0.3	89.9 $\pm$ 0.2	90.4 $\pm$ 0.0	92.7 $\pm$ 0.2	88.7 $\pm$ 0.1
<b>EN-DRO</b>	95.2 $\pm$ 0.6	91.0 $\pm$ 0.1	91.4 $\pm$ 0.1	93.7 $\pm$ 0.1	89.8 $\pm$ 0.1
<b>CreDRO</b>	<b>97.1<math>\pm</math>0.3</b>	<b>92.5<math>\pm</math>0.1</b>	<b>92.4<math>\pm</math>0.1</b>	<b>96.1<math>\pm</math>0.1</b>	<b>90.9<math>\pm</math>0.2</b>
CreWra	96.1 $\pm$ 0.2	91.5 $\pm$ 0.2	91.5 $\pm$ 0.1	95.0 $\pm$ 0.1	89.9 $\pm$ 0.1
CreRL <sub>1.0</sub>	94.6 $\pm$ 0.3	91.7 $\pm$ 0.1	91.5 $\pm$ 0.1	95.7 $\pm$ 0.2	90.1 $\pm$ 0.1
CreEns <sub>0.0</sub>	95.4 $\pm$ 0.3	91.1 $\pm$ 0.2	91.2 $\pm$ 0.1	94.7 $\pm$ 0.1	89.7 $\pm$ 0.1
CreDE	94.1 $\pm$ 0.4	91.8 $\pm$ 0.1	90.9 $\pm$ 0.1	95.0 $\pm$ 0.1	89.4 $\pm$ 0.2
Ensemble Number $M = 20$					
DE	94.8 $\pm$ 0.3	90.0 $\pm$ 0.2	90.6 $\pm$ 0.0	92.9 $\pm$ 0.3	88.9 $\pm$ 0.1
<b>EN-DRO</b>	95.7 $\pm$ 0.0	91.1 $\pm$ 0.1	91.6 $\pm$ 0.1	94.0 $\pm$ 0.1	90.0 $\pm$ 0.1
<b>CreDRO</b>	<b>97.4<math>\pm</math>0.1</b>	<b>92.7<math>\pm</math>0.1</b>	<b>92.5<math>\pm</math>0.1</b>	<b>96.4<math>\pm</math>0.0</b>	<b>91.1<math>\pm</math>0.1</b>
CreWra	95.7 $\pm$ 0.3	91.6 $\pm$ 0.1	91.6 $\pm$ 0.0	95.2 $\pm$ 0.0	89.0 $\pm$ 0.1
CreRL <sub>1.0</sub>	94.8 $\pm$ 0.3	91.8 $\pm$ 0.2	91.6 $\pm$ 0.1	95.7 $\pm$ 0.2	88.9 $\pm$ 0.2
CreEns <sub>0.0</sub>	95.5 $\pm$ 0.1	91.3 $\pm$ 0.0	91.4 $\pm$ 0.1	94.9 $\pm$ 0.1	88.8 $\pm$ 0.0
CreDE	94.3 $\pm$ 0.3	91.8 $\pm$ 0.0	91.2 $\pm$ 0.0	95.1 $\pm$ 0.2	88.4 $\pm$ 0.1

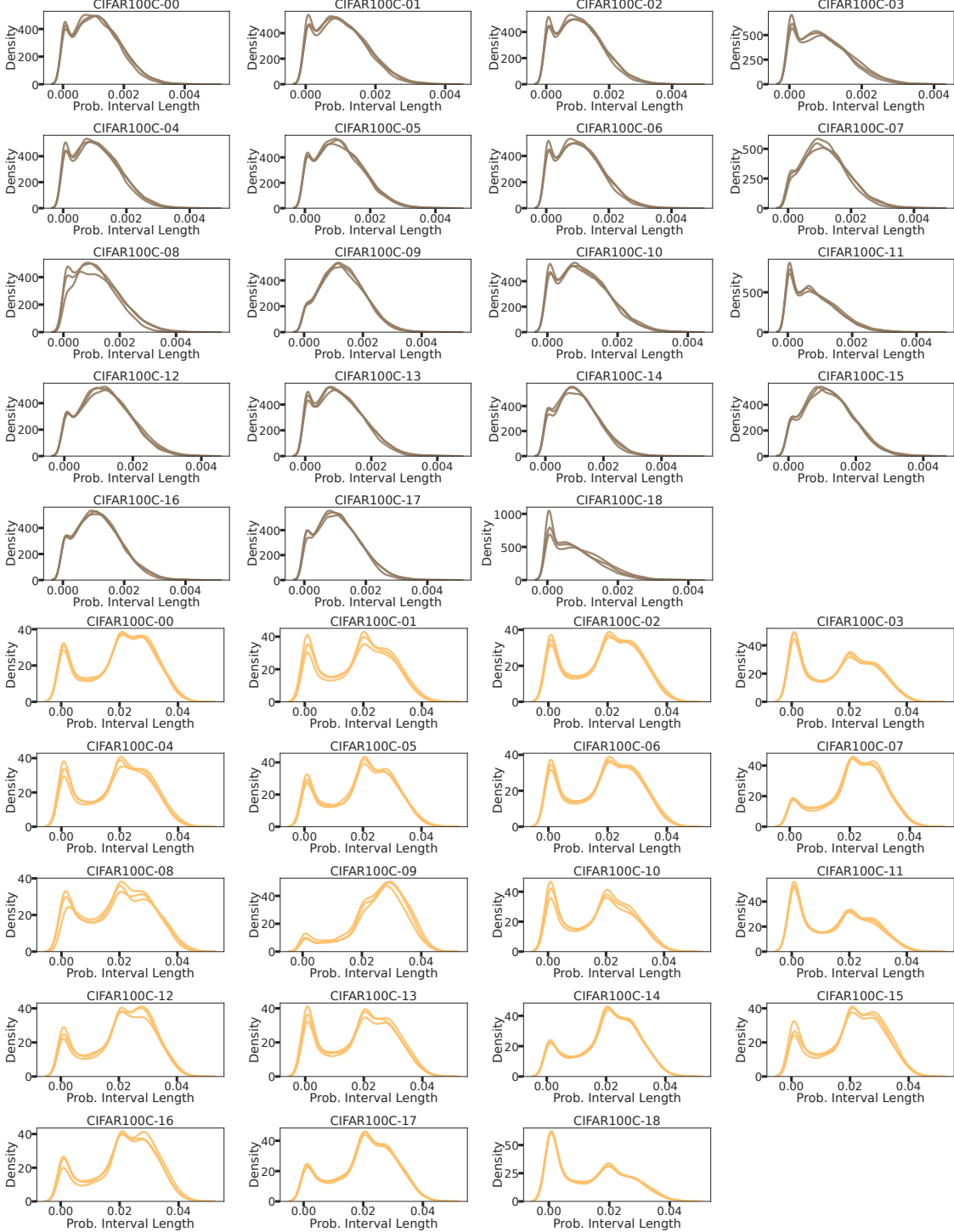


**Figure 7:** Kernel density plots of the averaged probability interval length (PIL) over classes on CIFAR100-C datasets with 19 types of corruptions: CreDE (top) and CreDRO (bottom). The averaged PIL for an input instance is computed as  $\text{PIL} = \frac{1}{100} \sum_{k=1}^{100} \bar{p}_k - \underline{p}_k$ . The results show that the PIL produced by CreDE is approximately 10 times tighter than that of CreDRO, which makes solving the optimization problem in (10) for EU estimation considerably more difficult. This is because, as the intervals become tighter (i.e., narrower bounds), the feasible region shrinks, often forcing the optimizer to search within a smaller, more constrained domain that frequently lies near or on the boundaries. This typically leads to more active constraints, worsened problem conditioning, and an increase in the number of iterations required for convergence.

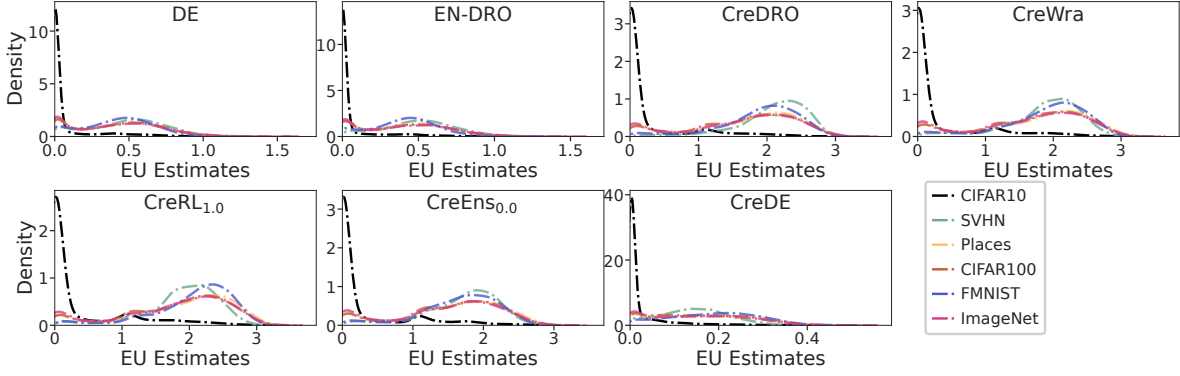


**Figure 8:** Kernel density plots of EU estimates on ID and OOD data from distinct methods. (ensemble size:  $M = 10$ ; first-run results)

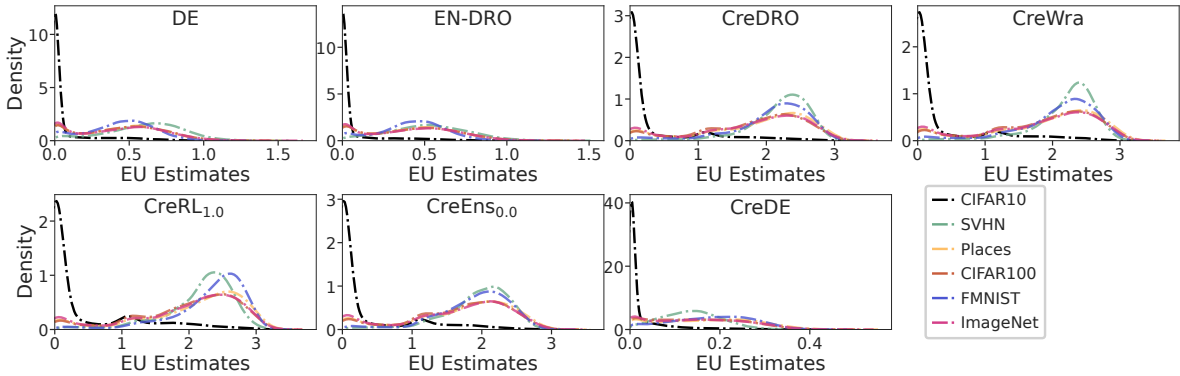


**Figure 9:** Kernel density plots of EU estimates on ID and OOD data from distinct methods. (ensemble size:  $M = 15$ ; first-run results)

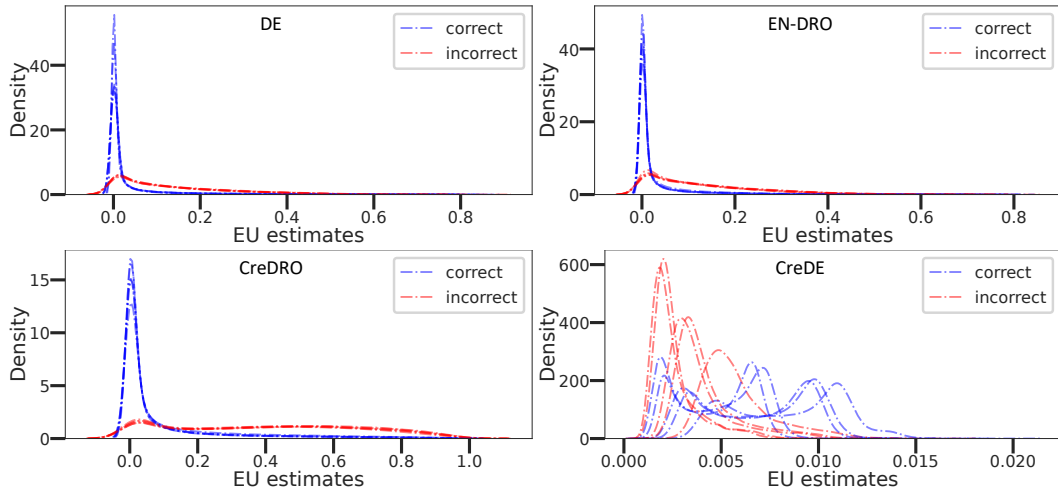


**Figure 10:** Kernel density plots of EU estimates on correctly and incorrectly classified medical test samples, across different classifiers. The plots show that CreDRO produces noticeably higher EU values for incorrectly classified samples than for correctly classified ones, qualitatively confirming its reliable EU estimation. In contrast, CreDE tends to be overconfident (overall smaller EU values) and struggles to distinguish between incorrectly and correctly classified samples.

## D Ablation study on training hyperparameter $\delta_G$

As shown in the Table 4, CreDRO’s performance is stable across different choices of  $\delta_G$ . This is because  $\delta_G$  reflects only one subjective belief from the model trainer about the worst-case scenario. In contrast, CreDRO training incorporates multiple subjective member beliefs about the potential distributional divergence (6), which reduces the significant impact of selecting a specific  $\delta_G$ . For example, an example showing how the selection of  $\delta_G$  influences CreDRO training is provided in Table 9.

**Table 9:** Example of the effect of  $\delta_G$  selection on CreDRO training. Ensemble size  $M = 5$ .

$\delta_G$	Individuals’ $\{\delta_i\}_{i=1}^5$ per Member	Number of Selected Top $\delta$ Samples per Batch
0.5	0.50, 0.625, 0.75, 0.875, 1.00	64, 80, 96, 112, 128
0.7	0.70, 0.775, 0.85, 0.925, 1.00	89, 99, 108, 118, 128
0.9	0.90, 0.925, 0.95, 0.975, 1.00	115, 118, 121, 124, 128

A smaller value of  $\delta_G$ , which reflects a more pessimistic belief about potential distribution divergence, may produce larger box credal sets. To empirically examine this effect, we use the averaged probability interval length (PIL) as a measure of the credal set size [Löhr et al., 2025], defined as follows:

$$\text{PIL} = \frac{1}{C} \sum_{k=1}^C \bar{p}_k - \underline{p}_k. \quad (12)$$

A larger value of PIL approximately indicates a larger credal set. We do not adopt the entropy-based EU measure because it only indirectly reflects the credal set size, and credal sets with different sizes may yield similar (or identical) values [Hüllermeier et al., 2022]. As shown in Figure 11, smaller values of  $\delta_G$  generally lead to larger box credal sets, confirming that increasing pessimism about distribution divergence results in wider probability intervals.

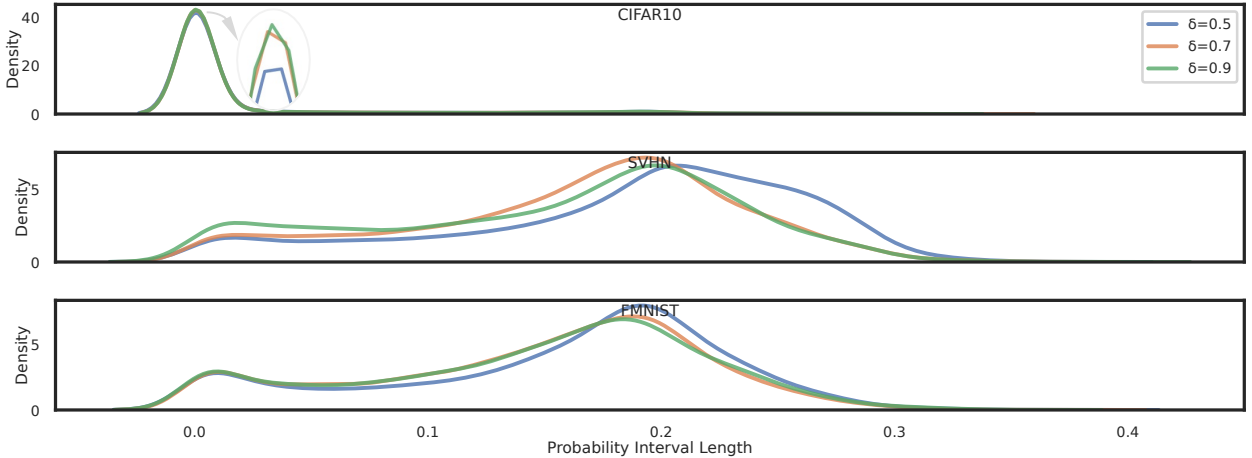


**Figure 11:** Kernel density plots of the averaged probability interval length (PIL) over classes on different datasets. The results empirically show that larger values of  $\delta_G$  generally lead to larger box credal sets.

## E Computational cost of epistemic uncertainty quantification

### E.1 Box credal set vs convex hull credal set

In this section, we analyze the computational cost of estimating epistemic uncertainty by computing the difference between the upper and lower entropy [Abellán et al., 2006] over two types of credal sets derived from softmax probability samples  $\{\mathbf{p}_i\}_{i=1}^M$  for  $C$  classes. Namely, we consider the box credal set  $\mathcal{K}_B$ , defined as

$$\mathcal{K}_B = \left\{ \mathbf{p} \mid p_k \in [\underline{p}_k, \bar{p}_k], \quad \sum_{k=1}^C p_k = 1 \right\},$$

where the upper and lower probability bound per class ( $\bar{p}_k$  and  $\underline{p}_k$ ) can be obtained from (7), and the convex hull credal set  $\mathcal{K}_C$ , defined by

$$\mathcal{K}_C = \left\{ \sum_{i=1}^M \pi_i \mathbf{p}_i \mid \pi_i \geq 0, \sum_{i=1}^M \pi_i = 1 \right\}.$$

**Box credal set case.** Let  $H(\mathbf{p}) := \sum_{i=1}^C -p_i \log p_i$  denote the entropy function over any valid probability vector. The optimizations for computing the *upper entropy* and *lower entropy* take the following forms:

$$\begin{aligned} & \text{maximize}_{\mathbf{p}} H(\mathbf{p}) \quad \text{s.t. } p_k \in [\underline{p}_k, \bar{p}_k] \quad \text{and } \sum_{k=1}^C p_k = 1 \\ & \text{minimize}_{\mathbf{p}} H(\mathbf{p}) \quad \text{s.t. } p_k \in [\underline{p}_k, \bar{p}_k] \quad \text{and } \sum_{k=1}^C p_k = 1 \end{aligned} \quad (13)$$

The optimization is performed over  $\mathbf{p} \in \mathbb{R}^C$  with  $C$  box constraints and one equality constraint. The objective  $H(\mathbf{p})$  is strictly concave. In practice, we use `scipy.optimize.minimize` with bounds and equality constraints, initialized at the mean probability vector, as shown in Figure 12 (left). Regarding the computational complexity, each iteration requires  $O(C)$  operations to compute the entropy and its gradient. The number of iterations  $T_B$  depends on the solver and problem conditioning. Therefore, the total complexity per instance is  $O(T_B C)$ , which depends only on the number of classes  $C$  and is independent of the number of samples  $M$ .

**Convex hull credal set case.** The convex hull credal set  $\mathcal{K}_C$  corresponds to convex combinations of the original  $M$  softmax samples. The optimizations for computing the *upper entropy* and *lower entropy* take the following forms:

$$\begin{aligned} & \text{maximize}_{\boldsymbol{\pi} \in \Delta^{M-1}} H\left(\sum_{i=1}^M \pi_i \mathbf{p}_i\right) \\ & \text{minimize}_{\boldsymbol{\pi} \in \Delta^{M-1}} H\left(\sum_{i=1}^M \pi_i \mathbf{p}_i\right) \end{aligned} \quad (14)$$

where  $\boldsymbol{\pi} \in \mathbb{R}^M$  lies in the  $M$ -simplex  $\Delta^{M-1}$ . The objective in (14) is concave in  $\boldsymbol{\pi}$  and is optimized using `scipy.optimize.minimize` with  $M$  box constraints  $\pi_i \in [0, 1]$  and one equality constraint  $\sum_{i=1}^M \pi_i = 1$ . The full implementation is shown in Figure 12 (right). Regarding the computational complexity, each function evaluation involves computing the convex combination  $\mathbf{p} = \sum_{i=1}^M \pi_i \mathbf{p}_i$  at a cost of  $O(MC)$ , plus an entropy evaluation costing  $O(C)$ . Each iteration thus costs  $O(MC)$ , with the total number of iterations  $T_C$  depending on the solver and problem conditioning, resulting in a total complexity of  $O(T_C MC)$  per instance. The complexity scales linearly with both the number of classes  $C$  and the number of samples  $M$ .

**Summary of computational trade-offs.** From the analysis above, we observe that box credal set methods provide a more efficient alternative, with complexity that does not depend on  $M$ . This

is particularly advantageous when the number of softmax samples  $M$  is large, since optimizing the convex hull upper entropy becomes computationally expensive in that case. Note that computing the lower entropy remains inexpensive for both methods: for  $\mathcal{K}_B$ , the minimum occurs at an extreme point of the box, while for  $\mathcal{K}_C$ , it is attained at one of the original samples. A summary of the computational complexities for entropy optimization is given in Table 10.

**Table 10:** Summary of computational complexities for entropy optimization.  $T_B, T_C$  denote the number of iterations of the numerical optimizer.

Quantity	Problem Size	Complexity per Instance
Box $\mathcal{K}_B$	upper entropy	$C$ variables
Box $\mathcal{K}_B$	lower entropy	$C$ variables
Convex hull $\mathcal{K}_C$	upper entropy	$M$ variables
Convex hull $\mathcal{K}_C$	lower entropy	trivial

```

import numpy as np
from scipy.optimize import minimize
from scipy.stats import entropy
from tqdm import tqdm
def upper_entropy(probs: np.ndarray, base: float = 2) -> np.ndarray:
    """Compute the upper entropy of a box credal set.
    Args:
        probs: numpy.ndarray of shape (n_instances, n_samples, n_classes)
        base: float, default=2
    Returns:
        ue: numpy.ndarray of shape (n_instances,)
    """
    def fun(x: np.ndarray) -> np.ndarray:
        return -entropy(x, base=base)

    x0 = probs.mean(axis=1)
    constraints = {"type": "eq", "fun": lambda x: np.sum(x) - 1}
    ue = np.empty(probs.shape[0])
    for i in tqdm(range(probs.shape[0])):
        bounds = list(zip(np.min(probs[i], axis=0), np.max(probs[i], axis=0), strict=False))
        res = minimize(fun=fun, x0=x0[i], bounds=bounds, constraints=constraints)
        ue[i] = -res.fun
    return ue

def lower_entropy(probs: np.ndarray, base: float = 2) -> np.ndarray:
    """Compute the lower entropy of a box credal set.
    Args:
        probs: numpy.ndarray of shape (n_instances, n_samples, n_classes)
        base: float, default=2
    Returns:
        le: numpy.ndarray of shape (n_instances,)
    """
    def fun(x: np.ndarray) -> np.ndarray:
        return entropy(x, base=base)
    MINIMIZE_EPS = 0.001
    x0 = probs.mean(axis=1)
    # If the initial solution is uniform, slightly perturb it, as minimize will fail otherwise
    uniform_ids = np.all(np.isclose(x0, 1 / probs.shape[2]), axis=1)
    x0[uniform_ids, 0] += MINIMIZE_EPS
    x0[uniform_ids, 1] -= MINIMIZE_EPS

    constraints = {"type": "eq", "fun": lambda x: np.sum(x) - 1}
    le = np.empty(probs.shape[0])
    for i in tqdm(range(probs.shape[0])):
        bounds = list(zip(np.min(probs[i], axis=0), np.max(probs[i], axis=0), strict=False))
        res = minimize(fun=fun, x0=x0[i], bounds=bounds, constraints=constraints)
        le[i] = res.fun
    return le

```

```

import numpy as np
from scipy.optimize import minimize
from scipy.stats import entropy
from tqdm import tqdm
def upper_entropy_convex_hull(probs: np.ndarray, base: float = 2) -> np.ndarray:
    """Compute the upper entropy of a convex hull credal set.
    Args:
        probs: numpy.ndarray of shape (n_instances, n_samples, n_classes)
        base: float, default=2
    Returns:
        ue: numpy.ndarray of shape (n_instances,)
    """
    def fun(w: np.ndarray, extrema: np.ndarray) -> np.ndarray:
        prob = w @ extrema
        return -entropy(prob, base=base)

    w0 = np.ones(probs.shape[1]) / probs.shape[1]
    constraints = {"type": "eq", "fun": lambda x: np.sum(x) - 1}
    bounds = [(0, 1)] * probs.shape[1]
    ue = np.empty(probs.shape[0])
    for i in tqdm(range(probs.shape[0])):
        res = minimize(fun=fun, args=probs[i], x0=w0, bounds=bounds, constraints=constraints)
        ue[i] = -res.fun
    return ue

def lower_entropy_convex_hull(probs: np.ndarray, base: float = 2) -> np.ndarray:
    """Compute the lower entropy of a convex hull credal set.
    Args:
        probs: numpy.ndarray of shape (n_instances, n_samples, n_classes)
        base: float, default=2
    Returns:
        le: numpy.ndarray of shape (n_instances,)
    """
    def fun(w: np.ndarray, extrema: np.ndarray) -> np.ndarray:
        prob = w @ extrema
        return entropy(prob, base=base)

    w0 = np.ones(probs.shape[1]) / probs.shape[1]
    constraints = {"type": "eq", "fun": lambda x: np.sum(x) - 1}
    bounds = [(0, 1)] * probs.shape[1]
    le = np.empty(probs.shape[0])
    for i in tqdm(range(probs.shape[0])):
        res = minimize(fun=fun, args=probs[i], x0=w0, bounds=bounds, constraints=constraints)
        le[i] = res.fun
    return le

```

**Figure 12:** Code implementation for computing the entropy difference of the box credal set (left) and the convex hull credal set (right), following Löhr et al. [2025].

## E.2 Empirical analysis of effect of interval tightness on optimization runtime for $\mathcal{K}_B$

In our implementation, the upper and lower entropy over  $\mathcal{K}_B$  are computed using `scipy.optimize.minimize` with box constraints and a simplex equality constraint, as discussed in Appendix E.1. The runtime depends non-monotonically on the width of the probability intervals. When the intervals are moderately tight, the feasible region is small, and the initialization at the mean probability vector is typically close to the optimum, which could lead to fast convergence in a few iterations. For wide intervals, the optimizer explores a larger feasible region and requires more iterations. Conversely, when the intervals become extremely tight, the feasible polytope may become nearly degenerate, with many active bound constraints interacting with the normalization constraint. This can lead to ill-conditioning and slower convergence for SLSQP-style solvers. Empirically, Table 11 reports the averaged probability interval length (PIL) on the CIFAR10 test data of several credal classifiers and their UQ runtime. CreDRO achieves the fastest regime, while too-tight probability intervals of CreDEs lead to a higher UQ computation cost.

**Table 11:** Averaged probability interval length (PIL =  $\frac{1}{10} \sum_{k=1}^{10} \bar{p}_k - \underline{p}_k$ ) and UQ runtime (seconds) on CIFAR10 test instances.

	PIL (Run #1)	PIL (Run #2)	PIL (Run #3)	Averaged UQ Runtime
CreDRO	0.0179 $\pm$ 0.0498	0.0180 $\pm$ 0.0501	0.0182 $\pm$ 0.0506	116.37 $\pm$ 0.30
CreWra	0.0216 $\pm$ 0.0557	0.0207 $\pm$ 0.0539	0.0212 $\pm$ 0.0551	123.83 $\pm$ 0.24
CreRL <sub>1.0</sub>	0.0271 $\pm$ 0.0636	0.0274 $\pm$ 0.0643	0.0263 $\pm$ 0.0633	133.31 $\pm$ 1.04
CreDE	0.0009 $\pm$ 0.0025	0.0009 $\pm$ 0.0025	0.0009 $\pm$ 0.0025	165.20 $\pm$ 0.96

## F Possible extension to regression

In this section, we illustrate a possible way of formulating credal predictions from our CreDRO in regression settings.

Note that the training framework is in principle applicable to regression, as the training objective  $\mathcal{L}(\cdot, \cdot)$ , outlined in Algorithm 1, could be any suitable loss, provided it enables neural networks to produce probabilistic predictions. E.g., the Gaussian negative log-likelihood loss [Lakshminarayanan et al., 2017] for regression tasks.

In a regression setting with a continuous target space  $\mathbb{R}$ , our analysis considers a set of Gaussian predictions produced by an ensemble, denoted  $\{\mathcal{N}(\mu_i, \sigma_i^2)\}_{i=1}^M$ . Gaussian distributions are chosen because mean-variance neural network estimators are relatively straightforward to learn from data and widely applied in practice [Lakshminarayanan et al., 2017, Sluijterman et al., 2024, Lehmann et al., 2024]. In this setting, the final single precise prediction is approximated by a single Gaussian distribution, denoted as  $\mathcal{N}(\mu_G, \sigma_G^2)$ , constructed by matching the mean and variance of the corresponding mixture distribution [Lakshminarayanan et al., 2017]. The resulting mean is given by  $\mu_G = M^{-1} \sum_{i=1}^M \mu_i$ , and the variance is computed as

$$\sigma_G^2 = \frac{1}{M} \sum_{i=1}^M (\sigma_i^2 + \mu_i^2) - \mu_G^2. \quad (15)$$

Under the context of a continuous target space, extracting probability intervals over discrete classes as in (7) is not applicable. Consequently, CreDRO could map the ensemble's Gaussian predictions,  $\{\mathcal{N}(\mu_i, \sigma_i^2)\}_{i=1}^M$ , to a finitely generated credal set [Augustin et al., 2014, Chau et al., 2025b]. This credal set  $\mathcal{K}_F$  is defined as

$$\mathcal{K}_F = \left\{ \sum_{i=1}^M \pi_i \mathcal{N}(\mu_i, \sigma_i^2) \mid \pi_i \geq 0, \sum_{i=1}^M \pi_i = 1 \right\}. \quad (16)$$

Hence,  $\mathcal{K}_F$  represents a set of mixtures of Gaussians. When  $\pi_i = M^{-1}$  for all  $i$ ,  $\mathcal{K}_F$  reduces to the final prediction  $\mathcal{N}(\mu_G, \sigma_G^2)$  in classical ensembles [Lakshminarayanan et al., 2017], given by (15).

From the above analysis, the way of applying credal predictions of our CreDRO in regression demonstrates promising potential. However, compared to classification, credal methods for uncertainty quantification in regression remain less mature, with fewer studies on uncertainty measures and their evaluation protocols. Therefore, more rigorous theoretical analysis and more comprehensive empirical validation in regression are left for future work.